JOURNAL OF GEOPHYSICAL RESEARCH, VOL. 115, D06204, doi:10.1029/2009JD012055, 2010

RF and X-ray source locations during the lightning attachment process

J. Howard,[1] M. A. Uman,[1] C. Biagi,[1] D. Hill,[1] J. Jerauld,[1,2] V. A. Rakov,[1] J. Dwyer,[3] Z. Saleh,[3] and H. Rassoul[3]

Received 13 March 2009; revised 13 October 2009; accepted 20 October 2009; published 18 March 2010.

[1] Using an eight-station array of electric field derivative (*dE*/*dt*) sensors and colocated NaI X-ray detectors, we have obtained 3-D RF source locations during the leaders and attachment processes of three first strokes initiated by stepped leaders in natural cloud-to-ground lightning and one stroke initiated by a dart-stepped leader in a rocket-and-wire triggered flash. Stepped leader and dart-stepped leader *dE*/*dt* pulses are tracked from a few hundred meters to a few tens of meters above ground, after which pulses of different characteristics than the step pulses are observed to occur at lower altitudes. These postleader pulses include: (1) the "leader burst," a group of pulses in the *dE*/*dt* waveform occurring just prior to the slow front in the corresponding return-stroke electric field waveform; (2) *dE*/*dt* pulses occurring during the slow front; and (3) the fast-transition or dominant *dE*/*dt* pulse that is usually associated with the rapid transition to peak in the return-stroke electric field waveform. Additionally, the timing coincidence between X rays and *dE*/*dt* pulses on colocated measurements is used to examine the X-ray production by the postleader processes. Leader bursts (LBs) are the largest X-ray producers of the three postleader processes and exhibit propagation speeds that exceed the preceding stepped leader speeds by more than an order of magnitude. Slow-front (SF) and fast-transition pulses appear to originate from similar physical processes, probably the multiple connections of upward and downward leaders. However, more X-rays are coincident with slow-front pulses than with fast-transition pulses.

Citation: Howard, J., M. A. Uman, C. Biagi, D. Hill, J. Jerauld, V. A. Rakov, J. Dwyer, Z. Saleh, and H. Rassoul (2010), RF and X-ray source locations during the lightning attachment process, *J. Geophys. Res.*, *115*, D06204, doi:10.1029/2009JD012055.

1. Introduction

[2] Approximately 90% of all cloud-to-ground lightning is classified as downward negative lightning [*Rakov and Uman*, 2003]. These discharges involve one or more leader/return-stroke processes, commonly referred to as "strokes," in which the leader descends from the cloud, lowering negative charge toward the earth, and the return stroke propagates up the leader channel from near ground level to the cloud, draining to ground the charge previously deposited on the leader channel. Leaders of downward negative lightning are classified into two primary categories: (1) stepped leaders, which propagate through virgin air in a discontinuous, branched, and tortuous manner at an average speed of the order of 10^5 m s^{-1} and typically precede the first return stroke in a flash; and (2) dart leaders, which appear to propagate in a more or less continuous manner through a preconditioned channel (warm, low density, and partially ionized air left by a previous lightning process) at a speed of the order of 10^7 m s^{-1} and generally precede subsequent return strokes in a flash. Occasionally, a dart leader traveling down a previously formed channel will reach a region that has decayed beyond the level of preconditioning that can sustain the continuous propagation; consequently, the leader will continue from that point on in a manner more like that of a stepped leader, however, with shorter steps and inter-step time. These leaders are termed dart-stepped leaders and typically propagate at a speed of the order of 10^6 m s^{-1}. When any leader approaches within tens or hundreds of meters of ground, one or more upward positive leaders are initiated from nearby objects on the ground or from the ground, signifying the beginning of a transition from the leader phase to the return-stroke stage. This transition, commonly referred to as the attachment process, involves the downward leader and a particular upward positive leader, known as the "upward connecting leader," accelerating toward each other, resulting in a connection, which may consist of multiple branches, and launching the current waves, both upward and downward, that constitute the return stroke [e.g., *Jerauld et al.*, 2007]. Many of the physical mechanisms involved with leader propagation, the attachment process, and the resulting return stroke occur on a microsecond or submicrosecond timescale and therefore have remained poorly documented and hence poorly understood.

[1]Department of Electrical and Computer Engineering, University of Florida, Gainesville, Florida, USA.
[2]Now at Raytheon Missile Systems, Tucson, Arizona, USA.
[3]Department of Physics and Space Sciences, Florida Institute of Technology, Melbourne, Florida, USA.

0148-0227/10/2009JD012055

[3] Researchers have employed various methods and equipment to study the downward leader, attachment, and return-stroke processes. The use of streak-camera techniques [e.g., *Schonland*, 1956; *Berger and Vogelsanger*, 1966; *Orville and Idone*, 1982; *Jordan et al.*, 1992] has allowed investigators to compile statistics about the propagation speed, step length, and interstep interval for different types of leaders. Generally, low-luminosity upward connecting leaders and the rapid processes of the attachment phase are unresolved using these techniques; however, some of these studies, along with still photography [e.g., *Golde*, 1967; *Orville*, 1968; *Hagenguth*, 1947], have provided indirect evidence of upward connecting leaders. More recent studies, such as those using the Automatic Lightning Discharge Progressing Feature Observation System (ALPS) optical imaging system [*Yokoyama et al.*, 1990; *Wang et al.*, 1999, 2001], have imaged and estimated speeds for upward connecting leaders. Additionally, *Biagi et al.* [2009] presented high-speed video images that unambiguously identified an upward connecting leader for eight consecutive strokes in a rocket-triggered lightning flash, although no speed could be estimated for them. On the basis of the collection of optical data available, an upward connecting leader initiated in response to a downward-stepped leader is known to have a typical length of some tens of meters, although it may reach a few hundred meters in length if initiated from a tall structure. An upward connecting leader that is initiated in response to a downward-dart leader has a typical length on the order of 10 m or less.

[4] Return-stroke observations including current, electric and magnetic field, and electric and magnetic field-derivative waveforms have also provided important information about the nature of the attachment process. A number of researchers have reported measured characteristics for negative lightning first-return-stroke electric fields and/or field derivatives. Most of these measurements were performed at distances of some tens of kilometers from the lightning channel, allowing the radiation field component to dominate the overall electric field, and the field propagation was generally over seawater so that the field amplitude and shape were not significantly affected by propagation effects [e.g., *Weidman and Krider*, 1978; *Cooray and Lundquist*, 1982; *Murray et al.*, 2005]. *Lin et al.* [1979] measured and characterized negative first-stroke electric and magnetic fields at distances ranging from 1 to 200 km over land, and *Master et al.* [1984] reported some first-stroke electric fields ranging from 1 to 20 km. *Jerauld et al.* [2008] presented first-stroke electric and magnetic fields and field derivatives for 18 first return strokes each observed simultaneously at multiple distances ranging from less than 100 m to about 1 km. In most of these studies, involving the entire range of reported distances, the first-stroke electric and magnetic field waveforms are shown to exhibit a slow-front/fast-transition sequence. When the field propagation is over tens of kilometers of seawater, as observed by *Weidman and Krider* [1978], the distant first-stroke electric field is typically characterized by a gradual rise (slow front) to 0.4–0.5 of the peak value in several microseconds (2–8 μs), followed by a fast transition ($\sim$0.2 μs or less) to peak. In addition to distant first-stroke electric and magnetic fields, slow fronts and fast transitions have also been observed in first-stroke currents measured at instrumented towers [*Berger et al.*, 1975; *Eriksson*, 1978; *Visacro et al.*, 2004], close first-stroke electric and magnetic field and field-derivative measurements [*Jerauld et al.*, 2008], and in distant electric fields for subsequent strokes that were initiated by dart and dart-stepped leaders [*Weidman and Krider*, 1978]. For each waveform type, the qualitative description for the slow front and fast transition is similar; however, the slow front to peak value ratio and the time duration for both phases varies. *Jerauld et al.* [2007] recently reported an unusual triggered lightning stroke which produced current, electric field, and magnetic field waveforms, the latter two measured at 15 and 30 m, with a slow front and fast transition similar to that typically observed in natural-negative first-stroke currents and distant electric fields. On the basis of modeling results, which used the channel-base current as input, and comparisons with natural-negative first-stroke waveforms, *Jerauld et al.* [2007] argued that the physics behind the initial several-microsecond-duration "slow front" involves a pair of microsecond-duration current waves, each having a peak value up to some tens of kiloamperes, propagating in opposite directions from near the initial junction point of the descending stepped leader and the upward connecting leader, as the two leaders approach each other. The fast transition was also viewed as a pair of current waves, but resulting from the final connection of the leaders, which propagate away from the junction point in opposite directions.

[5] Recently, ground-based X-ray detection networks have provided new insights and raised new questions about the physics of leader propagation. It has been shown that both stepped and dart leaders produce X-ray emissions as they descend toward the ground [*Moore et al.*, 2001; *Dwyer et al.*, 2003, 2004, 2005]. Further, the production of X-rays in stepped leaders was shown to be associated with the step formation process [*Dwyer et al.*, 2005]. For both types of leaders, the emissions were first observed when the leaders were just several hundred meters above ground, terminated near the time of the return stroke, and were composed of multiple, brief bursts of X-rays in the 30–250 keV range, with each burst typically lasting less than 1 μs [*Dwyer et al.*, 2004, 2005]. *Howard et al.* [2008] reported that there was a close spatial (<50 m) and temporal (0.1–1.3 μs) association between the sources of the X-rays and causative leader step electric field change, and that this relationship was similar for both a stepped leader in a natural flash and a dart-stepped leader in a rocket-triggered flash. The similarities of the X-ray emissions from different types of leaders imply a common physical mechanism in all downward negative leaders and further imply that dart leaders, which are generally viewed as moving continuously, involve some degree of stepping. The mechanism by which leaders produce X-rays is a topic of active debate, but it likely involves the acceleration of high-energy electrons, known as runaway electrons, under the influence of strong electric fields in air [*Gurevich and Zybin*, 2001]. One of the currently favored proposed models is the so-called cold runaway breakdown mechanism [*Gurevich*, 1961; *Dwyer*, 2004; *Moss et al.*, 2006], which does not require an external source of energetic seed particles nor a strong electric field that extends for some tens to hundreds of meters in space, as does the Relativistic Runaway Electron Avalanche (RREA) mechanism [*Gurevich et al.*, 1992; *Lehtinen et al.*, 1999]. However, the cold runaway model does require the electric field near the step

formation to approach values equivalent to ~30 MV/m at standard air conditions, approximately 10 times the electric field required for conventional breakdown.

[6] Clearly, our present understanding of the stepping process and the associated X-ray production is incomplete. Among the questions currently being addressed are the luminosity (production rate) and energy spectrum of the source runaway electrons, the possible dosage of radiation near the source, the directionality and attenuation of the X-ray emissions, and the characteristics of the electric field at the leader front [*Saleh et al.*, 2009]. Further, it is presently unclear whether or not processes associated with the attachment and return-stroke phases contribute to the production of X-rays, one of the topics we investigate and resolve here. Answers to some of these questions can, in principle, be obtained by analyzing time-correlated measurements of close electric field, electric field derivative, and X-rays for sources with known locations, which served as the primary motivation for implementing a time-of-arrival (TOA) location system at the International Center for Lightning Research and Testing (ICLRT) [*Howard et al.*, 2008] to complement the existing close field and field derivative measurements of the Multiple Station Experiment (MSE) [e.g., *Jerauld*, 2007; *Jerauld et al.*, 2008] and the X-ray sensors of the Thunderstorm Energetic Radiation Array (TERA) [e.g., *Saleh et al.*, 2009]. More precisely, a TOA network was created using subsets of MSE and TERA measurements.

[7] The principle of operation for the TOA network is on the basis of that of previous lightning location systems such as the Lightning Detection and Ranging (LDAR) system [*Poehler and Lennon*, 1979; *Maier et al.*, 1995], Lightning Mapping Array (LMA) networks [*Rison et al.*, 1999; *Koshak et al.*, 2004, *Thomas et al.*, 2004], and the *dE*/*dt* network of *Thomson et al.* [1994]. The former two systems operate at VHF, while the latter was a wideband system. Each of these systems measures the arrival time of impulsive radiation from a lightning event at multiple stations and then uses the set of arrival times with TOA techniques (e.g., hyperbolic fixing, hyperplane approach, or a nonlinear least squares Marquardt algorithm) to locate the source of radiation. These systems map the spatial progression of lightning flashes and have useful applications in various studies, for example, determining storm charge structure, locating the initiation region of flashes, and measuring flash rates. Nevertheless, some of the properties generally shared by these networks make them ill-equipped for our purposes. First, the size of these networks is usually some tens of kilometers in diameter. On the basis of the error analysis presented by *Thomas et al.* [2004], the altitude uncertainty is dependent on the ratio of the horizontal distance between the source and the closest station to the height of the source. For large-area networks, the altitude uncertainty can easily exceed several hundred meters for sources within 1 km of ground. This accuracy is insufficient for tracking leaders within several hundred meters of ground, which is the typical leader height when X rays are first detected at ground, presumably due to the decreasing luminosity of energetic electrons with increasing leader altitude and the high attenuation ($\propto[\exp(-r/120)]/r$, where r is in meters) of X-rays in air [*Saleh et al.*, 2009]. Second, these TOA systems are typically automated to provide real-time display, so they only locate one source per some specified time interval (typically 80 μs). Since the duration of X-ray detection is typically less than a millisecond, fewer than a dozen sources would be provided during this interval. For these two reasons, we have designed our TOA network to cover a very small area (~0.25 km^2) and imposed no time interval constraint between source locations. Finally, we note that we use wideband (DC to 20 MHz, −3 dB) *dE*/*dt* antenna systems, similar to those used in the KSC TOA network of *Thomson et al.* [1994], as opposed to VHF receivers. *Howard et al.* [2008] have previously discussed the ICLRT TOA system for the location of lightning leader *dE*/*dt* pulses and X-ray emissions and have demonstrated the ability to locate, in three dimensions, stepped-leader step electric field changes and their associated X-ray sources.

[8] In this paper, we extend the study of *Howard et al.* [2008] to examine the location of *dE*/*dt* sources for the stepped leader, the attachment process, and the beginning of the return stroke for three natural-lightning first strokes and one triggered-lightning stroke. We utilize colocated X-ray sensors with time synchronization to determine the role of the attachment process and the return stroke in X-ray production, the role of stepped leader steps being relatively well documented [*Dwyer et al.*, 2005; *Howard et al.*, 2008]. The results represent the first study of the location and characteristics of electromagnetic sources following the stepped leader and associated with the attachment and return-stroke processes. The three postleader processes we study are as follows: (1) the "leader burst" just preceding the slow front in the electric field waveform, (2) the slow front pulses occurring during the slow front, and (3) the fast-transition pulse or dominant pulse in the *dE*/*dt* waveform resulting in the fast transition in the electric field waveform.

2. Experiment

[9] The experiment discussed here was performed during the 2006 and 2007 summer seasons at the ICLRT, University of Florida and Florida Institute of Technology-operated facility which occupies approximately 1 km^2 at the Camp Blanding Army National Guard Base in north-central Florida. A primary goal of this experiment was to investigate physical processes in nearby cloud-to-ground lightning by using data from the MSE and TERA measurements, hereafter referred to as the MSE/TERA network. By extension, these measurements include the ICLRT TOA system. The layout of the MSE/TERA network during the 2007 season is shown in Figure 1. At that time, the network consisted of 24 stations and over 60 sensors. Information about the MSE/TERA measurements used for this study is listed in Table 1. All signals were transmitted via Opticomm MMV-120C fiber-optic links to the Launch Control trailer (Figure 1), where the waveforms were filtered, digitized, and stored. The output of a field mill (measuring the quasi-static electric field at ground, which can be used as an indicator of cloud electrification) was monitored by a PC that automatically armed and disarmed the network when conditions were appropriate. The method of triggering the digitizers was dependent on whether a lightning was natural or rocket-triggered. For rocket-triggered lightning, data acquisition was triggered when the channel base current, measured by a 1 mΩ resistive shunt, exceeded a threshold (~6 kA). For natural lightning, the outputs from two optical sensors, which view the network at low altitude from

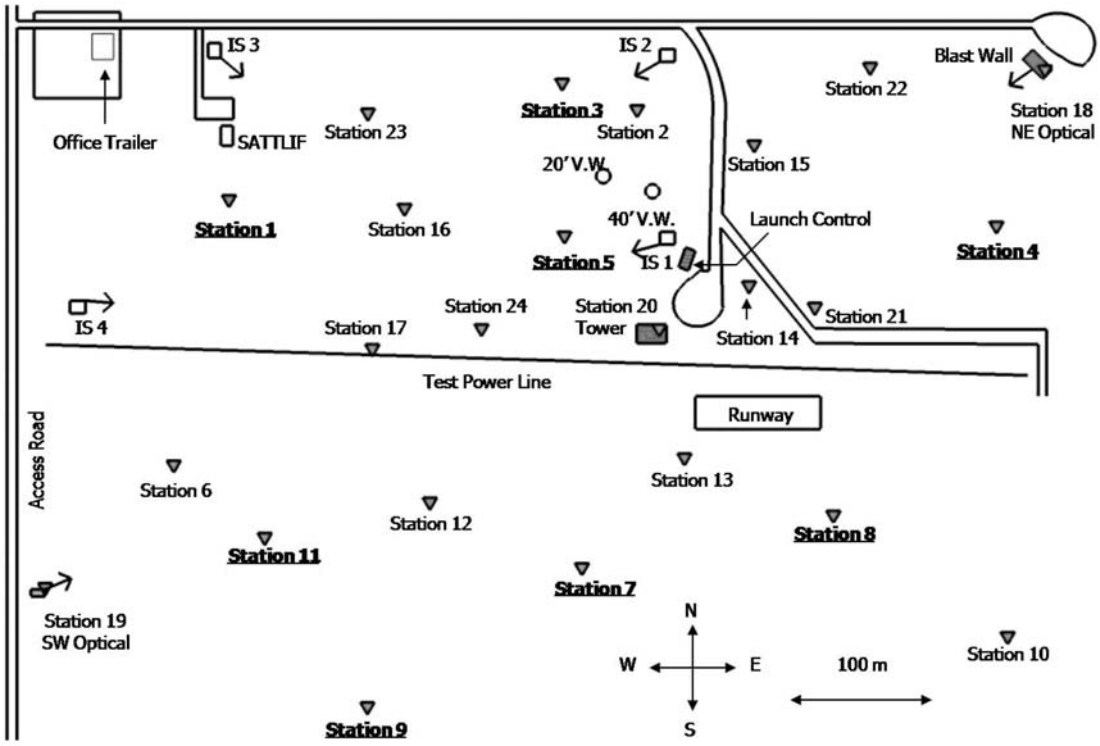

Figure 1. Layout of the MSE/TERA at the ICLRT as it existed in 2007. Each station is denoted with a triangular symbol and is labeled with its name. The names of the eight TOA stations are in underscored boldface.

opposite corners of the site (see Figure 1), were required to simultaneously exceed a threshold, so that the digitizers were triggered only for cloud-to-ground lightning within or very near the network. Note that natural flashes are documented using a "MSE-YYFF" nomenclature and rocket-triggered flashes are documented using the "UF-YYSS" nomenclature, where "YY" is the two-digit year for the flash, "FF" is the natural flash two-digit number for that year, and "SS" is a rocket-triggered shot attempt for that year.

[10] A video system, which is automated along with the rest of the network, was added to the MSE/TERA in 2006. The four-color CCD cameras comprising this system were placed in separate Instrument Station buildings (IS1–IS4 in Figure 1) across the site to optimize coverage of the network. These video signals were transmitted via fiber-optic links to Launch Control where they were time-stamped, converted to quadrature mode (images from four cameras viewed in one frame), and recorded on a Sony SR2000 TIVO digital video recorder. This system, while not providing high-spatial resolution, does provide information about the strike location, channel geometry, and stroke multiplicity. For rocket-triggered lightning, where the time and location of the flash are known, the video system was complemented with a Sony (DCR-TRV900) MiniDV camcorder and a Panasonic Lumix FZ-8 digital camera that operated in Motion Picture Mode, both located in the Launch Control trailer. Additionally, three Nikon 35-mm SLR cameras fitted with neutral density filters, set to automatically acquire a 6 s exposure with each rocket launch, were aimed at the launcher from different locations.

[11] The primary focus of this paper is the data obtained by an eight-station subset of the MSE/TERA that provides 3-D source locations for low-altitude lightning processes via the use of TOA techniques. The eight TOA stations are identified in Figure 1 in underlined boldface. Each of these stations was equipped with a wideband (DC to 20 MHz, −3 dB) flat-plate *dE*/*dt* antenna [see *Jerauld*, 2007; *Jerauld*

Table 1. Characteristics of the MSE/TERA Measurements Used for This Study

Sensor	Stations	Amplitude Range	Sampling Rate (MHz)	Record Length	Bandwidth
E field	2, 4, 5, 6, 9, 10	±85 kV m^{-1}	10	2 s	0.2 Hz[a]–3 MHz[b]
TOA *dE*/*dt*	1, 3, 4, 5, 7, 8, 9, 11	±30 kV m^{-1} μs^{-1}	250	8 segments, 2 ms each	DC to 20 MHz[b]
TOA X-ray	1, 3, 4, 5, 7, 8, 9, 11	6 MeV	250	2 segments, 2 ms each	See comment[c]
Optical	18, 19	+2 V	10	2 s	DC to 1 MHz[d]
Base current	20	±60 kA	100	10 segments, 1 ms each	DC to 8 MHz[e]

[a]Limited by the decay time constant of the integrating circuit.
[b]Limited by the digitizer.
[c]Response of X-ray detectors to single X-ray are usually specified in rise and fall times, in this case approximately 0.20 μs and 0.9 μs, respectively.
[d]Limited by the preamplifier.
[e]Limited by the current-viewing resistor (CVR).

et al., 2008] and a TERA box containing shielded and unshielded NaI/photomultiplier tube (PMT) detectors, similar to the system described by *Saleh et al.* [2009], the unshielded detectors being used in the TOA network. The locations of these sensors were accurately determined in a local coordinate system using an Electronic Total Station Traverse and a surveyor level. The origin of this coordinate system is near the southeast corner of the Office Trailer (Figure 1). Additionally, the transit time delay for each sensor was measured end-to-end with an accuracy of ~2 ns. Both the *dE*/*dt* and X-ray measurements were recorded on LeCroy four-channel digital storage oscilloscopes, sampled at 250 MHz for 2 ms with 1 ms of pretrigger. The TOA measurements were stored over four oscilloscopes, with one channel from each of these oscilloscopes being simultaneously recorded on a fifth oscilloscope in order to synchronize their timebases.

[12] The process of determining source locations begins with synchronizing the different oscilloscope timebases and cross-correlating the signals to identify common events across multiple channels. Arrival times are then selected using the positive peak of each *dE*/*dt* event. The set of arrival times selected for an event must all occur within a narrow window of time which is physically constrained by propagation paths and the transit time delays. Using this set of times, all combinations for $N \geq 5$ stations are used in a nonlinear least squares Marquardt algorithm, similar to that of *Thomas et al.* [2004] and *Koshak et al.* [2004], to determine the location and time of occurrence for the source. The final solution is selected on the basis of a metric of the smallest product of the reduced Chi-square value and location uncertainty of the solution. The location uncertainties (errors) used in this metric are predicted from the covariance matrix returned by the solution algorithm. These location errors vary from one source to another and are strongly dependent on the source location and the combination of stations utilized in the solution. For the four strokes analyzed here, the location uncertainties for the optimum solutions were often within 2–3 m in the horizontal directions and within 10 m in altitude for sources 50 m or more above ground. Both the optimum solutions and uncertainties are listed in Tables 2 and 3. Additional comments on location errors are found in section 4.4.

3. Data and Analysis

[13] The *dE*/*dt* records from three natural first strokes initiated by stepped leaders and one rocket-triggered lightning stroke initiated by a dart-stepped leader are presented in Figures 2, 3, 7, 8, 10, 12, 14, and 16–18. Figures 2, 3, 7, 8, 10, 12, 14, and 16–18 use the atmospheric electric sign convention, meaning an upward-directed electric field at ground level (equivalent to negative charge source directly overhead) corresponds to a negative field value. All records exhibited pulses associated with the stepping of a downward negatively charged leader as well as with processes following the leader phase. The postleader-phase processes produced pulses with different characteristics than those of the stepped-leader phase. We identify these postleader pulses as "leader bursts," "slow-front pulses," and "fast-transition pulses," the latter two occurring during the SF/fast-transition sequence generally associated with the return stroke and the former with a recently identified process apparently associated with the overall attachment process.

[14] In Figures 2–4, 7–14, and 16–18 and Tables 2 and 3 presented, *dE*/*dt* pulses are divided and labeled into groups. Groups of pulses occurring during the leader phase are typically characterized by a dominant bipolar pulse, identified as the primary leader step (LS), along with some smaller secondary pulses which are closely related in time (typically within 3 μs) and space (typically several meters in horizontal displacement; the vertical displacement is discussed later in more detail) to the primary leader step of the group. Groups of leader pulses are identified in Figures 2–4, 7–13, 16, and 17 and Tables 2 and 3 by capital letters, with ascending letters corresponding to later times. Groups of pulses occurring after the leader phase are classified into three general categories: (1) LB for "leader burst" pulses, (2) SF for pulses occurring during the slow front of the electric field and field derivative waveforms, and (3) FT for the "fast-transition" pulse, the dominant *dE*/*dt* pulse of the postleader phase. If necessary, pulses within each of the aforementioned groups are further distinguished by numeric identifiers, with increasing numbers corresponding to pulses occurring later in time. As noted earlier, information regarding TOA solutions is listed in Tables 2 and 3. For each solution, we give the local source coordinates (x, y, z), time of occurrence relative to trigger time (t), covariance estimates for the location uncertainties (Δx Δy Δz), the number of stations used in the solution (N), and a clarifier term to help identify the pulse within the group. The clarifiers used for leader-phase pulses denote one of three designations: (1) LS, indicating the primary leader step and typically the largest pulse of a group, as previously noted; (2) BS, indicating a secondary pulse occurring prior to the leader step; and (3) AS, indicating a secondary pulse occurring after the leader step. Finally, it is noted that Figures 2, 3, 7, 8, 10, 12, 14, and 16–18 depicting *dE*/*dt* waveforms (see above) have been correlated to align notable features and shifted so that the peak of the fast-transition pulse occurs at time zero; hence the actual times of occurrence (t) given in Tables 2 and 3 do not correspond directly with Figures 2, 3, 7, 8, 10, 12, 14, and 16–18.

[15] In addition to the *dE*/*dt* TOA analysis, we present the first analysis of colocated *dE*/*dt* and X-ray measurements to examine X-ray production because of low-altitude postleader processes. The basis of this analysis is the timing coincidence between X ray and *dE*/*dt* events as demonstrated for leader steps by *Howard et al.* [2008]. On the basis of the work of *Howard et al.* [2008], who found that X-rays associated with the leader phase follow the leader step *dE*/*dt* peak by 0.1–1.3 μs, an X-ray is deemed "coincident" with a *dE*/*dt* event when the X-ray is detected essentially simultaneous with or within ~1 μs following the *dE*/*dt* event. In this study, each pair of colocated measurements is synchronized to a common timebase and then examined for time coincidence between X-ray bursts and each of the three *dE*/*dt* postleader group types.

3.1. MSE-0604

[16] Flash MSE-0604, the designation indicating that it was the fourth natural flash recorded in the year 2006, occurred on 2 June 2006 at approximately 22:09 UT. First-stroke *dE*/*dt* waveforms from three stations of the network are shown in Figure 2. Although Figure 2, as well as others to be presented here, shows only the latter part of the leader

Table 2. Summary of TOA Location Results for the *dE*/*dt* Pulses Shown in Figures 2, 8, and 10 for the First Stokes of MSE-0604, MSE-0703, and MSE-0704, Respectively[a]

Pulse	Clarifier	x (m)	y (m)	z (m)	t (μs)	Δx (m)	Δy (m)	Δz (m)	N
				MSE-0604 2 June 2006					
A1	LS	256.5	−34.8	96.1	−73.472	0.4	0.9	2.2	5
B1	BS	227.3	−57.0	114.5	−70.146	2.2	5.8	11.2	5
B2	LS	238.4	−62.6	108.4	−70.012	1.7	3.1	6.0	7
B3	AS	239.1	−63.8	98.7	−69.022	0.2	0.5	0.9	5
C1	LS	242.3	−18.3	91.9	−61.139	0.2	0.4	0.7	6
C2	AS	243.1	−18.2	81.9	−60.364	0.8	2.6	4.1	6
D1	BS	239.0	−33.1	70.7	−48.560	0.7	2.2	4.3	5
D2	BS	245.6	−28.5	83.4	−48.374	0.4	1.0	1.7	5
D3	LS	244.9	−32.4	86.4	−48.303	0.8	1.1	1.7	5
D4	AS	252.2	−34.1	71.6	−46.185	0.5	1.1	2.2	5
E1	LS	240.0	−67.1	89.3	−41.835	0.5	0.6	1.0	5
F1	BS	237.0	−10.5	77.2	−33.733	0.5	1.3	1.9	5
F2	LS	241.8	−19.6	69.3	−33.505	0.6	1.4	2.4	7
G1	LS	257.1	−33.1	73.6	−26.627	0.2	0.4	0.8	6
H1	BS	237.6	−39.4	56.2	−24.472	0.2	0.6	1.4	5
H2	LS	237.8	−42.8	53.1	−24.299	0.1	0.4	0.7	5
I1	BS	235.5	−37.8	56.1	−21.828	0.5	1.0	2.4	6
I2	LS	237.8	−37.9	52.7	−21.143	0.4	0.8	1.8	7
J1	LS	250.6	−83.4	75.1	−17.032	1.1	1.8	4.3	7
K1	BS	231.2	8.3	53.2	−12.985	0.7	3.5	5.8	5
K2	BS	234.9	−1.1	59.1	−12.290	0.8	1.9	3.3	5
K3	LS	234.7	−3.1	56.2	−10.351	0.6	1.4	2.6	7
LB1		247.1	−32.0	45.1	−7.574	0.4	0.5	1.1	5
LB2		247.2	−34.0	33.9	−7.380	0.4	0.8	2.4	6
LB3		241.4	−33.0	18.9	−7.129	0.4	1.4	7.7	6
LB4		224.7	25.6	10.3	−6.994	0.8	1.8	29.6	6
SF1		222.0	29.9	8.1	−6.637	1.0	3.2	23.4	5
SF2		221.3	28.5	26.5	−6.423	3.4	5.1	7.5	5
				MSE-0703 14 July 2007					
A1	BS	591.2	−384.2	48.9	−41.869	0.9	0.8	1.7	6
A2	LS	592.2	−388.0	52.4	−41.755	0.3	0.2	0.4	5
B1	LS	590.6	−378.6	44.4	−29.376	0.8	0.9	1.4	5
C1	LS	586.0	−377.0	33.5	−25.400	4.0	4.4	9.3	6
D1	LS	578.2	−372.0	41.7	−15.181	12.1	13.1	21.8	5
LB1		586.0	−380.7	26.9	−14.147	10.2	11.3	30.6	6
LB2		592.2	−386.3	16.4	−13.791	6.8	8.0	35.7	5
SF		592.4	−381.7	31.3	−12.164	1.6	1.6	15.7	5
FT		592.9	−381.2	34.5	−11.963	2.2	1.9	19.5	5
AFT		591.0	−383.2	12.9	−11.509	5.7	6.2	40.5	6
				MSE-0704 16 July 2007					
A1	LS	−130.8	−120.9	104.8	−56.111	3.1	0.9	1.8	5
B1	LS	−117.0	−130.6	80.4	−39.283	13.0	3.7	7.4	5
B2	AS	−131.1	−122.0	67.6	−37.682	3.9	1.2	2.7	5
C1	LS	−107.7	−136.7	54.4	−24.381	10.9	3.3	9.5	5
C2	BS	−86.9	−102.0	97.8	−23.810	6.1	2.4	3.7	5
C3	BS	−62.9	−112.0	88.7	−23.486	9.6	3.8	6.6	5
C4	AS	−120.2	−131.2	59.1	−22.674	4.6	1.4	3.8	5
C5	AS	−118.0	−131.9	41.6	−21.373	13.1	3.8	14.2	5
D1	LS	−66.0	−91.3	94.2	−18.639	8.1	3.7	4.9	5
SF1		−123.7	−140.1	38.4	−15.326	39.0	10.3	42.2	5
SF2		−106.2	−131.2	29.8	−14.851	26.1	9.3	25.0	5
FT		−125.7	−134.6	28.9	−14.235	31.6	8.9	40.5	6

[a]Each event is identified by its pulse name and a clarifier, as discussed in the text. The results for each event include the local source coordinates (x, y, z), time of occurrence relative to trigger time (t), covariance estimates for the location uncertainties (Δx Δy Δz), and the number of stations used in the solution (N).

phase up to the return stroke, analysis was performed on the entire waveforms (~1000 μs prior to the return stroke) to locate *dE*/*dt* pulse sources associated with various leader branches and to determine the leader speed. The records from MSE-0604 were the most complex and also provided the most TOA locations of the four strokes analyzed here. Early in the waveforms of this stroke (prior to the portion shown in Figure 2), multiple regions of *dE*/*dt* activity, corresponding to stepped-leader branches separated by some hundreds of meters, were located by the network. The region of stepped-leader activity that ultimately connected with ground became the dominant source of *dE*/*dt* activity approximately 500 μs prior to the return stroke when it was about 350 m above ground. Over the next several hundred microseconds, this dominant region of leader activity continued extending downward as multiple branches. These branches were typically some tens of meters in length although one distinct branch did extend over a hundred meters in a generally horizontal direction.

[17] The *dE*/*dt* waveforms in Figure 2 show approximately the final 70 μs prior to the first return stroke of MSE-0604. TOA solutions for the pulses shown in Figure 2 are listed in

Table 3. Summary of TOA Location Results for the *dE*/*dt* Pulses of UF-0707 on 31 July 2007 Shown in Figure 12[a]

Pulse	Clarifier	x (m)	y (m)	z (m)	t (μs)	Δx (m)	Δy (m)	Δz (m)	N
A1	LS	381.8	−204.0	129.1	−17.366	3.4	3.1	16.7	5
B1	BS	384.8	−201.6	106.4	−12.933	1.8	1.7	10.1	5
B2	LS	388.0	−204.2	106.6	−12.505	2.9	2.7	15.8	5
B3	AS	386.9	−201.1	110.8	−12.056	6.2	5.7	33.0	5
B4	AS	390.1	−203.8	105.6	−11.611	7.1	6.4	37.9	5
C1	BS	387.6	−201.1	87.5	−9.554	2.1	1.9	13.1	5
C2	BS	390.2	−198.9	89.4	−8.781	0.9	0.8	5.3	5
C3	LS	392.7	−195.0	89.7	−7.730	5.6	5.0	34.2	5
C4	AS	389.2	−197.5	76.8	−7.120	5.6	5.2	39.6	5
LB1		389.2	−199.4	74.4	−4.358	1.8	1.7	13.1	5
LB2		389.6	−198.0	69.4	−4.141	2.9	2.7	22.4	5
LB3		390.4	−196.9	49.3	−3.939	3.9	3.7	40.9	5
SF1	Shoulder	387.7	−198.2	35.5	−1.171	0.5	0.5	7.4	5
SF2		388.8	−199.0	41.4	−1.002	1.9	2.0	24.5	5
SF3		392.7	−197.5	46.8	−0.818	2.1	2.1	23.5	5
SF4		390.7	−204.1	53.6	−0.572	4.5	4.5	43.3	5
FT		388.3	−203.5	55.6	−0.012	2.8	2.8	26.0	5

[a]Each event is identified by its pulse name and a clarifier, as discussed in the text. The results for each event include the local source coordinates (x, y, z), time of occurrence relative to trigger time (t), covariance estimates for the location uncertainties (Δx Δy Δz), and the number of stations used in the solution (N).

Table 2, as are the TOA solutions for the other two natural-lightning strokes presented. From Table 2, the leader-phase pulses (Groups A–K) of MSE-0604 clearly exhibited a tendency to decrease in altitude (z) with increasing time. Also observed from the solutions is the fact that pulses within each group tended to be closely spaced, while groups of pulses, perhaps associated with leader stepping in different branches, were often separated by some tens of meters, including displacement in directions parallel to the ground surface. It follows from the pulse group observations that leader steps are not necessarily the result of a singular breakdown, producing a singular radiation electric field emission; rather, leader steps frequently appear to be the result of a complex series of breakdowns which manifest itself as a "group" of pulses in the *dE*/*dt* records. Figure 2 illustrates the variety of waveforms that can be produced by leader steps. For instance, Group A illustrates a simple leader step signature; basically a fast, single, bipolar pulse

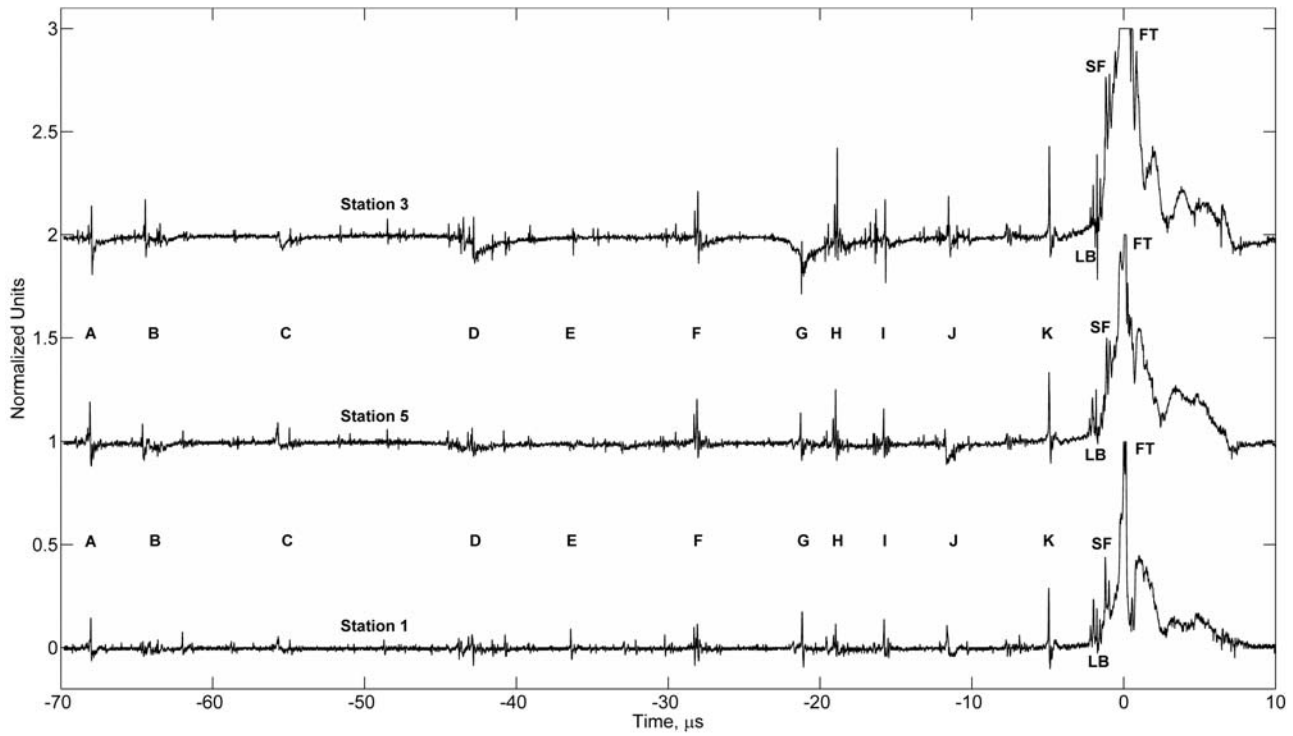

Figure 2. The *dE*/*dt* waveforms from the three stations closest to the first stroke of MSE-0604. This stroke exhibited the most active stepped leader and the most pronounced leader burst (LB) of the strokes analyzed here. The fast transition pulse could not be located because of saturation (limited by oscilloscope settings) at too many stations.

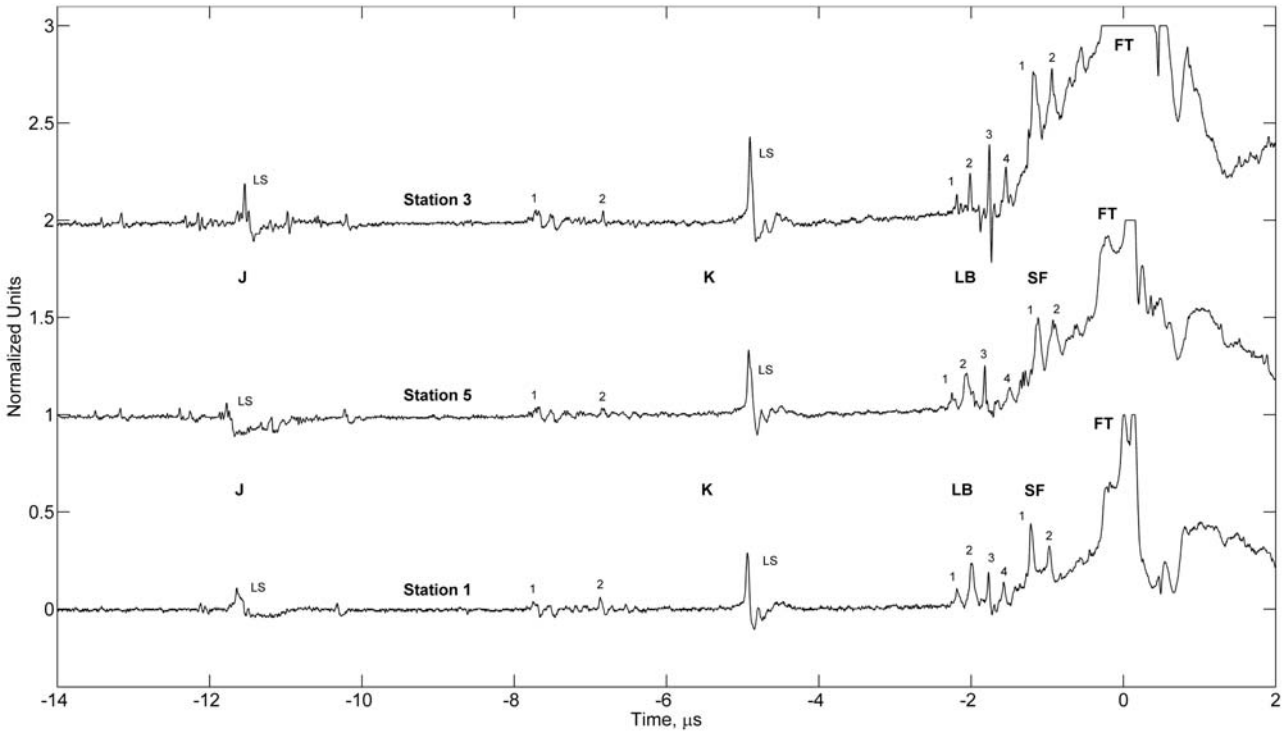

Figure 3. Zoomed view of the waveforms shown in Figure 2. This highlights the final leader steps and the postleader processes.

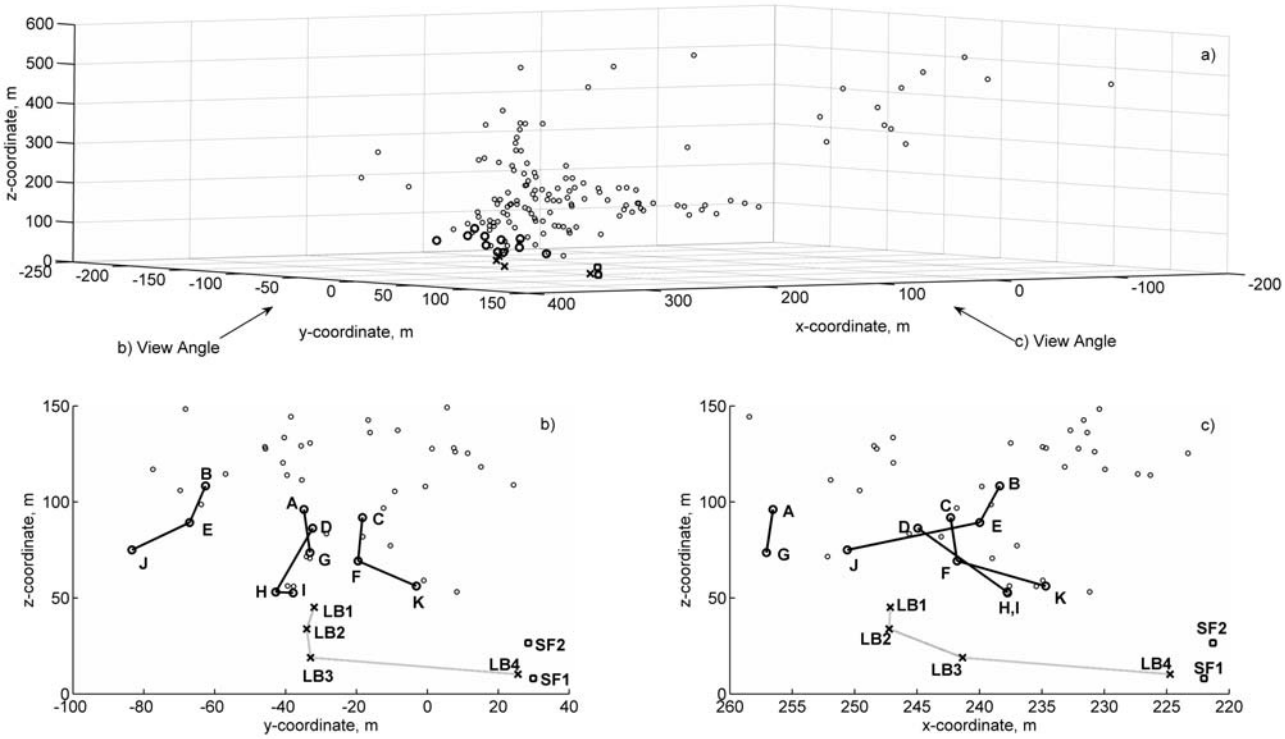

Figure 4. Visual representation of the first stroke in MSE-0604. (a) All located sources in a 3-D space. (b and c) Orthogonal vantage points, as indicated by the arrows, on an expanded scale to highlight the events in Table 2. Solid lines highlight patterns of movement by sequential leader groups, with the bold circles corresponding to the dominant pulses (LS) of those groups. The dotted line is used to highlight the sequential order of pulses in the LB. Slow-front (SF) pulses are indicated with the square symbols.

that is initially of positive polarity and followed by a slow decay from negative polarity back to the zero level. On the other hand, Groups D, H, and I are more complex leader steps that are characterized by a dominant bipolar pulse, similar to Group A, but with an accompanying series of secondary pulses.

[18] As the stepped leader of MSE-0604 neared the ground, waveform features different from the leader steps occurred, corresponding with the transition from the stepped-leader phase to the return-stroke phase. The waveforms of Figure 2 are expanded in Figure 3 to highlight the *dE*/*dt* activity occurring during this transition. Following the final leader step (Group K), a small gradual rise, which is most notable in Figure 2, was observed on the two closest *dE*/*dt* waveforms (stations 3 and 5), but not on any of the more distant stations. Approximately 2 μs after this rise began (around -2.3 μs in Figure 3), a burst of four *dE*/*dt* pulses, termed here a ''leader burst'' (LB) to distinguish it from the characteristic leader step *dE*/*dt* pulses, was observed. This quick burst of pulses has been previously observed by *Jerauld et al.* [2007] (referred to there as a burst of pulses) in close field waveforms at the ICLRT, and it is likely related to the pulses reported by *Murray et al.* [2005] (also termed a leader burst) in distant radiation field waveforms that propagated tens of kilometers over salt water. The termination of the leader burst coincides with the start of the initial rising portion of the *dE*/*dt* (and *E* field) waveforms, the so-called ''slow front'' of the return stroke [e.g., *Jerauld et al.*, 2007, 2008]. Shortly after the leader burst, a pair of relatively large pulses superimposed on the slow front was observed in the *dE*/*dt* waveforms, termed here SF pulses, which are similar in shape to but smaller in amplitude than the following fast-transition pulse. After the SF pulses, the gradual rise of the slow front continues until the onset of the rapid rise of the fast-transition pulse.

[19] Figure 4 utilizes the TOA solutions obtained by the network to produce a graphical representation of MSE-0604. In Figure 4a, all of the sources located for this stroke are plotted to emphasize the overall channel geometry detected by the network. Each source that occurred during the leader phase is represented by a circular plot symbol, with the bold circles corresponding to the dominant leader step (LS) pulses identified in Figure 2 and Table 2. The pulses of the LB are represented by 'X' symbols, and the SF pulses are denoted by square symbols. Figures 4b and 4c provide orthogonal 2-D views on an expanded scale to highlight the events that are identified in Figure 2. The symbol notation for Figures 4b and 4c is identical to that used in Figure 4a; however, some lines and group identifiers are added to highlight the progression of events in the last 70 μs prior to the return stroke. The solid lines connecting the bold circles are used to denote consistent patterns of movement made by sequential leader step (LS) pulses. Each of these connected symbols is labeled with its corresponding group identifier. The gray line in Figures 4b and 4c is used to highlight the sequential pattern of movement made by the pulses of the LB. The SF pulses, represented by the square symbols, are also labeled but are not connected by any line.

[20] On the basis of the representation in Figure 4, the leader pulses observed in Figure 2 corresponded with the stepped leader descending as four distinct branches down to an altitude between 50 and 75 m. The last *dE*/*dt* pulse of the leader phase, Group K, happened to be the final step in the leader branch that was nearest a tree-line bordering the north side of the research site at approximately $y = 20$ m. We hypothesize that the electric field from this step enhanced an upward positive leader from the tree line, which manifested itself as the small gradual rise observed only at the two closest stations. The LB, which was observed directly after this small rise, appears to have coincided with a process that quickly advanced from underneath the leader branches toward the tree line. Indeed, the pulses of the LB descended over 30 m in altitude and traversed a horizontal distance of about 60 m in less than a microsecond. Using the TOA locations in Table 2 for the LB pulses, the 3-D speeds between sequential events are calculated to be 5.9×10^7, 6.4×10^7, and 4.6×10^8 m s^{-1}; and the overall speed, from the first to last pulse, is approximately 1.2×10^8 m s^{-1}. Clearly, the calculated speed between the third and fourth pulses (4.6×10^8 m s^{-1}) is not physically possible. Because the distance between these two events is largely dominated by a horizontal component, which has estimated uncertainties of only a meter or so (Table 2), the LB may have involved two areas of simultaneous activity(perhaps some interaction between an upward and downward leader), rather than a process propagating from the location of LB3 to the location of LB4. Interestingly, both SF pulses of this stroke were located near the final pulse of the LB, although the vertical uncertainties of LB4, SF1, and SF2 were 10–30 m (Table 2). The locations determined for the SF pulses were within 10 m horizontally of a pine tree, about 7 m in height, which was struck and eventually killed by this flash. Unfortunately, records from too many stations, including all of those shown in Figure 3, were saturated during the fast transition so that a location for the fast-transition pulse could not be obtained.

[21] The TOA network allows an estimation of the downward velocity of the primary stepped-leader channel within several hundred meters of ground. To exclude laterally developing branches from the calculation, we selected a 60×60 m^2 plan view area underneath the dominant region of leader activity and included only the leader sources (no postleader sources) that occurred in the volume above it. Figure 5 shows the points which were included in this calculation, with the selection area indicated by the large square outlined at ground level. All leader sources occurring above the selection area are denoted with plus symbols while the remaining leader sources are indicated with circular symbols; the postleader events are denoted by their usual symbols (see Figure 4). The altitudes for these selected points were plotted versus time and then fit with a simple linear regression, with the slope corresponding with the downward leader velocity. The stepped-leader velocity for this stroke was determined to be 5.5×10^5 m s^{-1} with a determination coefficient between altitude and time of 0.95, as indicated in the MSE-0604 plot of Figure 6. Notice that the lowest sources of the leader did tend to be slightly below the linear fit, indicating that the velocity may have increased slightly as the leader neared ground. Although the vertical uncertainties are larger for the LB pulses (10–30 m), it is worth noting that the 3-D speeds between sequential LB pulses have vertical components of 5.8×10^7, 6.0×10^7, and 6.4×10^7 m s^{-1}, approximately two orders of magnitude higher than the events in the stepped leader.

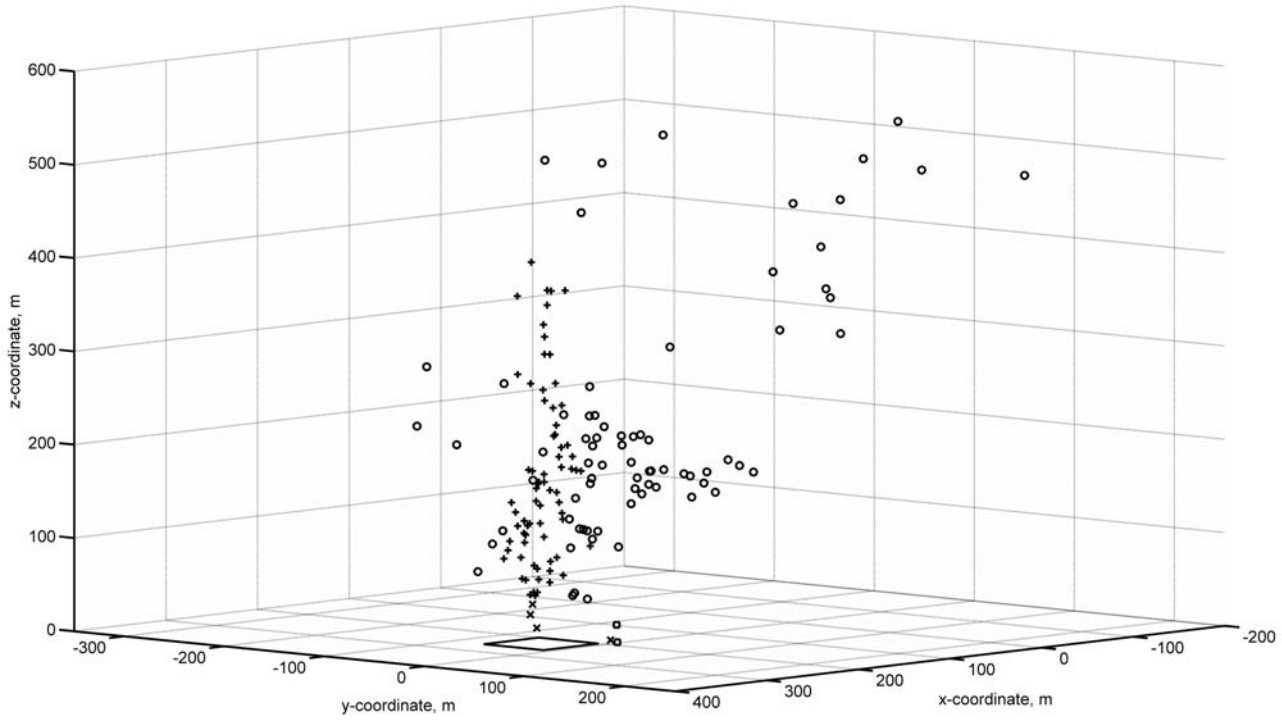

Figure 5. Illustration of points used in determining the downward velocity of the MSE-0604 stepped leader. To limit the effects of lateral branching, only the leader sources occurring above the square outline were used. These points are indicated with the plus symbols, while circles indicate all other leader points. The postleader events use the same symbols as Figure 4.

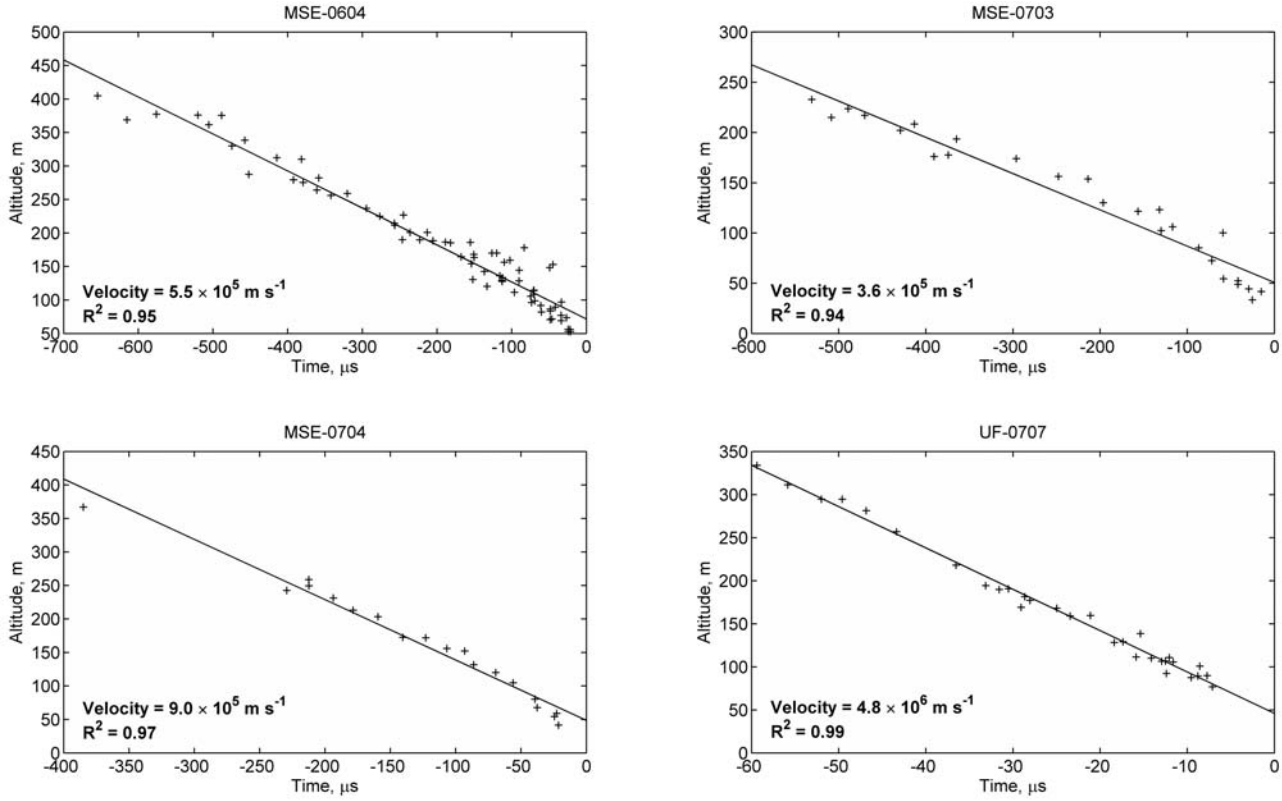

Figure 6. Determination of the downward leader velocity for each of the four strokes presented. Each plot indicates a strong linear dependence between leader altitude and time, with the slope corresponding to the velocity. The results for each linear fit are indicated in the appropriate plot.

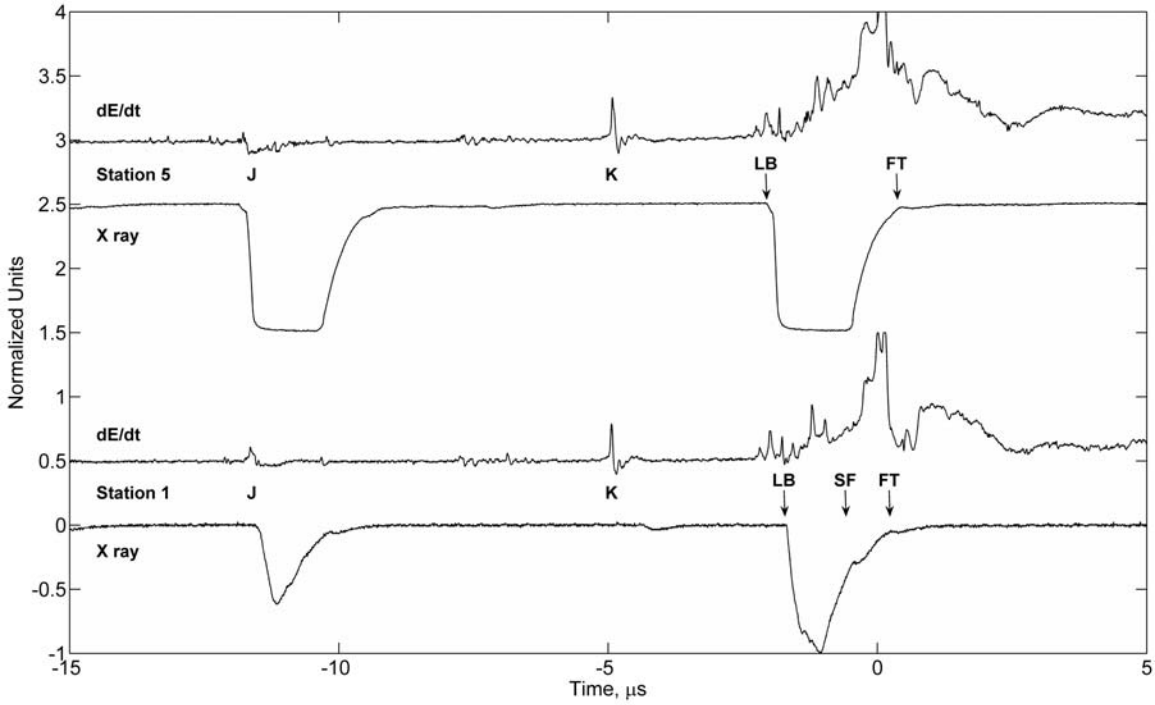

Figure 7. Two synchronized pairs of colocated X-ray and *dE*/*dt* measurements from MSE-0604. The time coincidence between these records is used to determine the association between X-rays and postleader *dE*/*dt* events. Note that the clipping of the X-ray pulses is because of the ±1 V range of the fiber-optic links.

[22] Finally, we report on the correlated X-ray and *dE*/*dt* observations obtained for this stroke using records from the colocated NaI/PMT detectors and *dE*/*dt* antennas. Figure 7 displays two pairs of these waveforms, with each pair being synchronized to a common timebase. In the PMT waveforms, X-rays arrive at the start of the negative going pulse. The pulse amplitude is dependent on the amount of energy deposited and the pulse shape is determined by the NaI light decay time and the RC time constant of the front-end electronics. The half-peak pulse width of a single X-ray burst is about 0.6 μs; therefore, the wide pulses shown in Figure 7 are the result of multiple X-ray bursts. Six stations, records from two of which are shown in Figure 7, allowed a comparison between *dE*/*dt* and X-ray events in the postleader waveforms. All six detected X-rays in association with the LB. Two of these six X-ray waveforms, including station 5 shown in Figure 7, were saturated during the SF pulses, preventing a comparison for this event. Of the four stations remaining, three, including station 1 shown in Figure 7, detected X-rays in association with the SF pulses. None of the six X-ray measurements were saturated at the time of the fast-transition pulse, allowing records from all six stations to be analyzed; three of them detected X-rays in association with the fast transition. For all stations, the X-ray burst associated with either the SF pulses or the fast transition was smaller than the X-ray burst from the LB process.

[23] Although the X-ray comparisons in this paper focus on the postleader events, it is interesting to note that Group K (around -5 μs in Figure 7), the final leader step, produced the largest *dE*/*dt* peak of the leader phase at each TOA station, except at station 3 where Group K was essentially matched by the peak of Group H, but the associated X-ray emission was one of the weakest detected during the leader phase of this stroke, barely detected by any of the TOA stations. The cause of this anomaly is currently unknown. It is possible that the proximity of Group K to the ground may have played some role in reducing the X-ray detection, but this view seems to be inconsistent with the copious X-rays detected from the LB, which was closer to ground than any of the leader steps. Figure 4 indicates that Group K was the final step in a leader branch that was propagating away from the sensors of the TOA network, but the additional atmospheric attenuation suffered by this relatively distant step is not significant enough to explain such a dramatic reduction in the deposited energy. These observations seem to indicate that the X-ray emissions may be beamed to some degree in the direction of the leader propagation; however, *Saleh et al.* [2009] reported that their observations of leader X-ray sources were most consistent with an isotropic source, at least in the lower hemisphere ahead of the leader tip. Since the emission's angular distribution in the upper hemisphere has yet to be determined (all the X-ray sensors are currently ground based), it is unclear what should be observed for a leader moving away from the network in a direction somewhat parallel to ground. Moreover, because of saturation of some of their sensors during low-altitude events, *Saleh et al.* [2009] could not rule out the possibility that the emissions become slightly beamed as the leader approaches very near the ground. Finally, it is noted that the X-ray production from Group K could have simply been less significant than other leader steps although the X-ray production generally increases as the leader nears ground; it appears that further study is warranted.

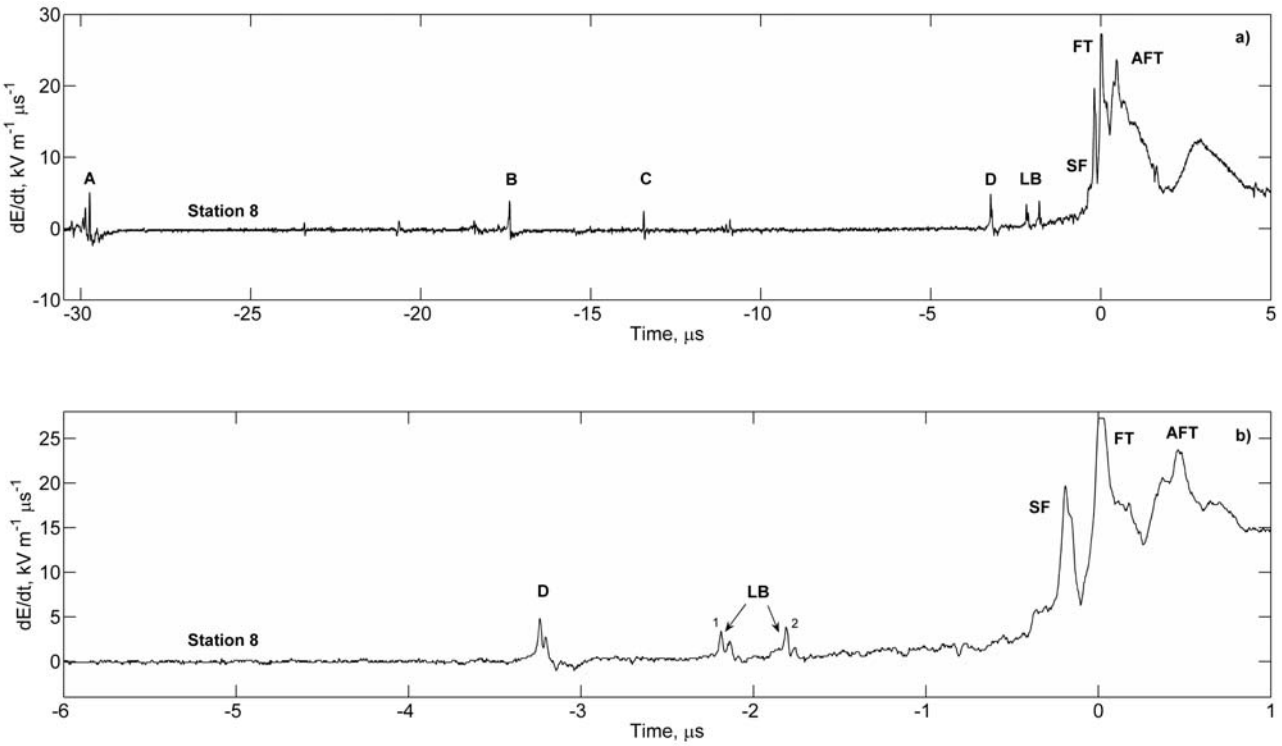

Figure 8. Closest *dE*/*dt* waveform to the first stroke of MSE-0703. (a) A relatively inactive leader for the final 30 μs prior to the return stroke. (b) A zoomed view of Figure 8a, which highlights a complex transition and attachment phase, which includes a LB and three significant pulses associated with the return stroke. The fast-transition (FT) pulse in this record is actually clipped because of saturation.

3.2. MSE-0703

[24] Flash MSE-0703 occurred on 14 July 2007 at about 16:25 UT. Figure 8 illustrates the final 30 μs of the closest *dE*/*dt* waveform (station 8) for this natural-lightning first stroke. The TOA solutions for the groups of pulses indentified in Figure 8 are listed in Table 2. A visual representation of this stroke, similar to the one for MSE-0604, is given in Figure 9. The symbol notation is the same as that used in Figure 4, but two additional plot symbols, which were not necessary before, are introduced: (1) a diamond symbol is used to denote the fast transition, and (2) a pentagram is used to denote a pulse unique to this stroke which occurred after the fast transition (labeled AFT). Overall, the leader phase of this stroke was much less active than that of MSE-0604. The TOA locations did reveal some leader activity that was horizontally separated by as much as a hundred meters; however, fairly little branching was observed in the channel that dominated the leader activity and ultimately connected with ground. The sources from this channel were used to calculate the downward leader velocity, which was found to be 3.6×10^5 m s^{-1} with a determination coefficient between altitude and time of 0.94. These data are presented in the MSE-0703 plot of Figure 6. Similar to MSE-0604, the final sources of the leader tend to be slightly below the fit, indicating an increase in velocity.

[25] Of primarily interest in this stroke are the events that occurred around the time of the return stroke. As seen in Figure 8, the final leader step, Group D, was followed by a pair of distinct pulses, identified here as the LB, which was then followed by the initiation of the slow front. It is unclear when exactly the slow front began because records from a few stations indicate that the LB may have included another pulse, following the two observed in Figure 8, although no location could be obtained for that pulse. Similar to the LB in MSE-0604, the TOA solutions for the LB indicate rapid downward and horizontal movement. The 3-D speed calculated for this LB is 3.8×10^7 m s^{-1} with the vertical component equal to 2.9×10^7 m s^{-1}, approximately two orders of magnitude faster than the stepped-leader downward velocity. We acknowledge that the separation of these sources is within their location uncertainties; however, the speed of this LB is consistent with the speeds calculated for the first three pulses of the MSE-0604 LB.

[26] Following the LB, the *dE*/*dt* waveform exhibits three large pulses occurring within a microsecond (Figure 8b). The first of these pulses is labeled a SF pulse primarily because it occurs after the start of the SF and prior to the dominant pulse (fast-transition pulse) of the return stroke *dE*/*dt* waveform. However, the appearance of this SF pulse is strikingly similar to that typically observed for a fast-transition pulse; a slow rising portion followed by a rapid transition to peak. A distinct feature of this SF pulse, compared with the other strokes presented here, is the absence of any appreciable period in which the waveform resumes its gradual rise prior to the dominant pulse. TOA solutions from Table 2 reveal that the SF pulse and the dominant pulse occurred at approximately the same location. Following the dominant pulse, there is one final pulse (AFT), similar in appearance to the previous two, before the field-derivative decays appreciably and gives rise to a subsequent hump. The presence of a pulse (AFT) following the dominant peak is not particularly common, but *Murray*

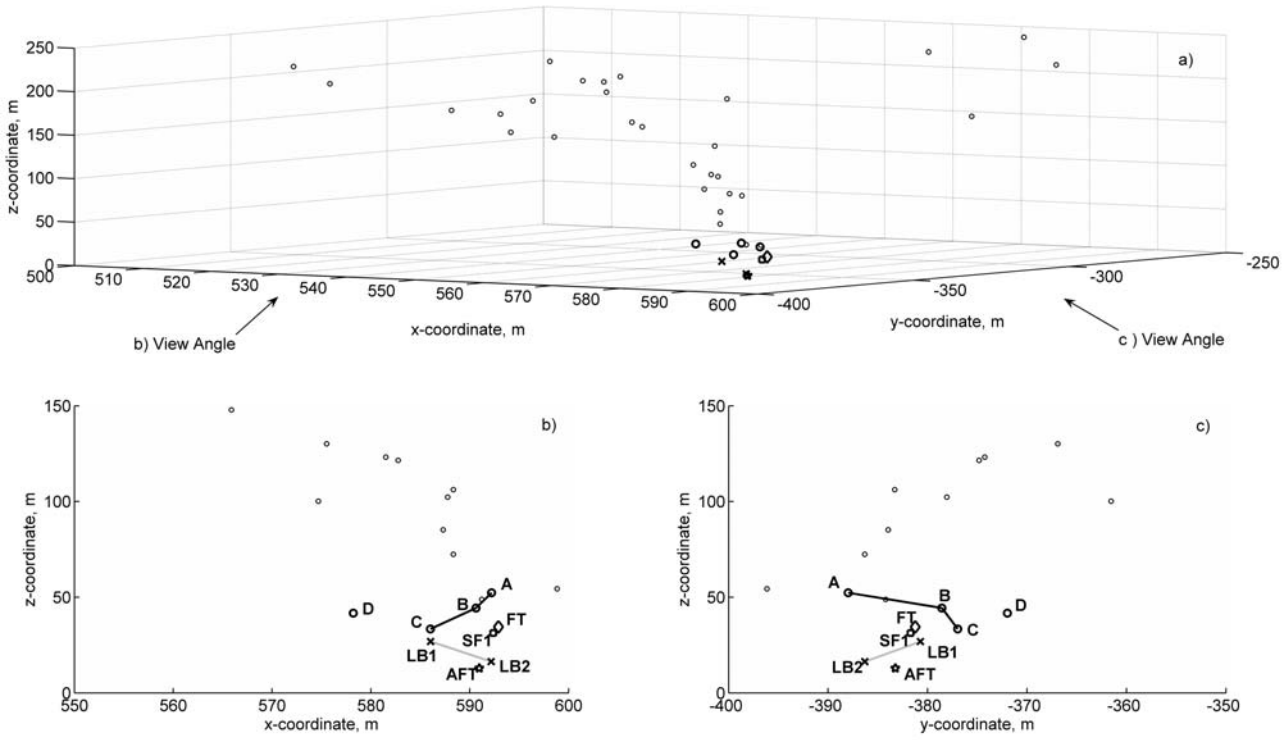

Figure 9. Visual representation of the first stroke in MSE-0703. The symbol notation is the same as that used in Figure 4 except two new symbols were added. The diamond corresponding to the fast-transition, and the pentagram denoting the pulse following the fast transition (AFT).

et al. [2005] did document some instances in their Type B events for distant first-stroke *dE*/*dt* waveforms. *Murray et al.* [2005] reported that 49 of 131 events (or 37%) produced 136 large pulses (in addition to the dominant peak) within ±1 μs of the dominant *dE*/*dt* pulse, although the pulses were nearly twice as likely to occur in the 1 μs prior to the dominant pulse as the 1 μs following the dominant peak. The final pulse of this stroke, which occurs after the fast-transition pulse, is unique to the waveforms presented here, so it is identified with a unique pulse label, AFT, in Table 2. The location of this final pulse is identified to be in the attachment region of this stroke and apparently lower than the SF and fast-transition pulses although the altitude errors for these three pulses are relatively large (SF, 16 m; FT, 20 m; and AFT, 41 m) because of their being so near the ground. Records from the video system for this flash confirm the general location of this stroke. The similarity in pulse shape, close temporal grouping, and proximity in location shared by the final three pulses of this stroke seem to indicate multiple occurrences of a common physical process.

[27] There were five stations available to make a comparison between the *dE*/*dt* pulses and X-rays occurring after the leader phase. All five detected X-rays in association with the LB. None of them detected X-rays with the slow front, and one of them detected X-rays in association with the fast transition. Interestingly, two of these five stations detected X-rays associated with the final pulse (AFT).

3.3. MSE-0704

[28] Flash MSE-0704, which occurred on 16 July 2007 at approximately 23:27 UT, is the third and final natural-lightning event to be presented. Two *dE*/*dt* waveforms illustrating the final 50 μs prior to the first return stroke of this flash are shown in Figure 10. TOA solutions for the pulses identified in Figure 10 are listed in Table 2. A graphical representation of this stroke is given in Figure 11, using the same symbol notation that was defined for the previous events. The TOA locations indicated that the leader activity of this stroke was loosely divided into two regions which were roughly separated by 100–200 m. This behavior is similar to that observed during the leader phase of the other natural-lightning strokes, except that the leader region that connected with ground did not clearly dominate the *dE*/*dt* activity of this stroke. These two regions produced approximately an equal number of sources and both exhibited a tendency for branching, typically some tens of meters in length. The downward leader velocity for this stroke was calculated using the sources from the leader region that connected with ground, excluding only a few points which extended horizontally out to Group D. As seen in the MSE-0704 plot of Figure 6, the downward leader velocity was determined to be 9.0×10^5 m s^{-1} with a determination coefficient between altitude and time of 0.97.

[29] An interesting feature of Figure 10 waveforms is the varying complexity displayed by the leader pulses. Several groups throughout the leader phase exhibited the simple leader-step signature typified by Group A, while others, such as Groups B and C, were much more complex. As was the case with previously examined stepped leaders, the pulses within each group tended to be closely spaced. An exception to this trend, however, was Group C which apparently corresponded with the simultaneous activity of two separate

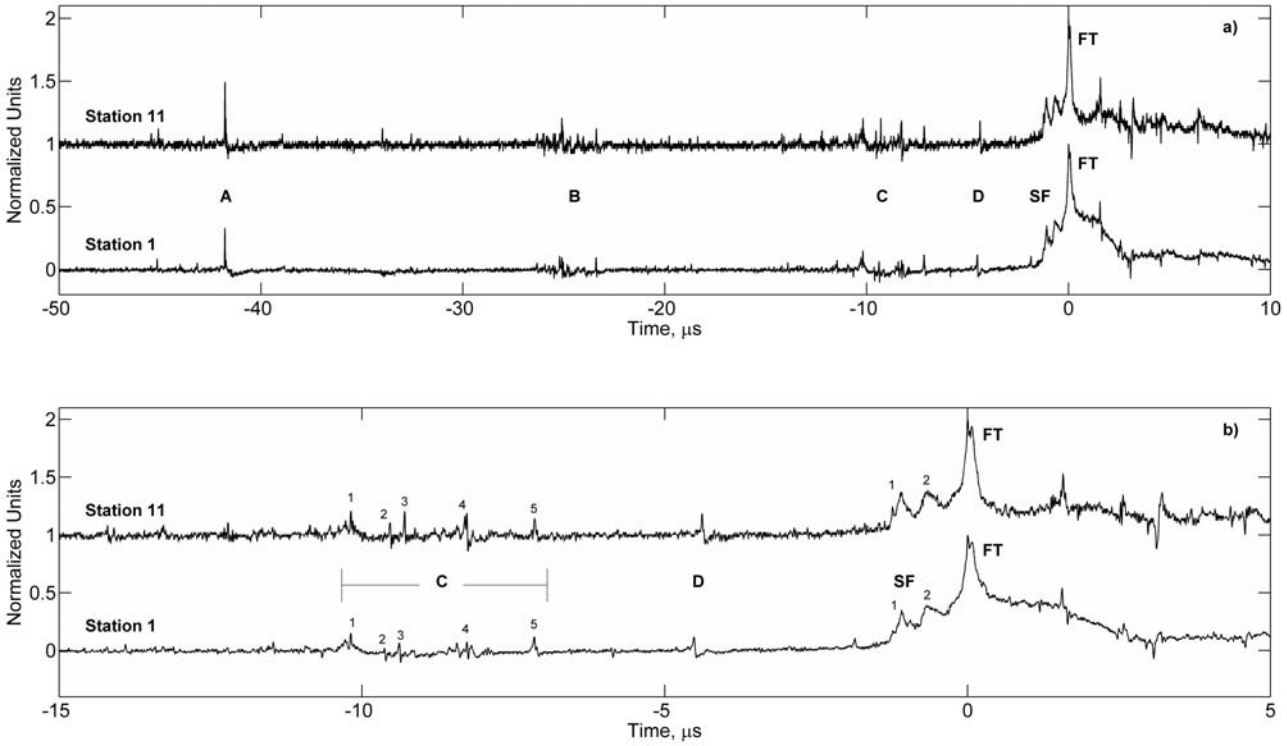

Figure 10. Two closest *dE*/*dt* waveforms for the first stroke of MSE-0704. (a) The leader is not particularly active, but involves some complex stepping signatures. (b) A zoomed view highlighting the final two leader steps and return-stroke activity.

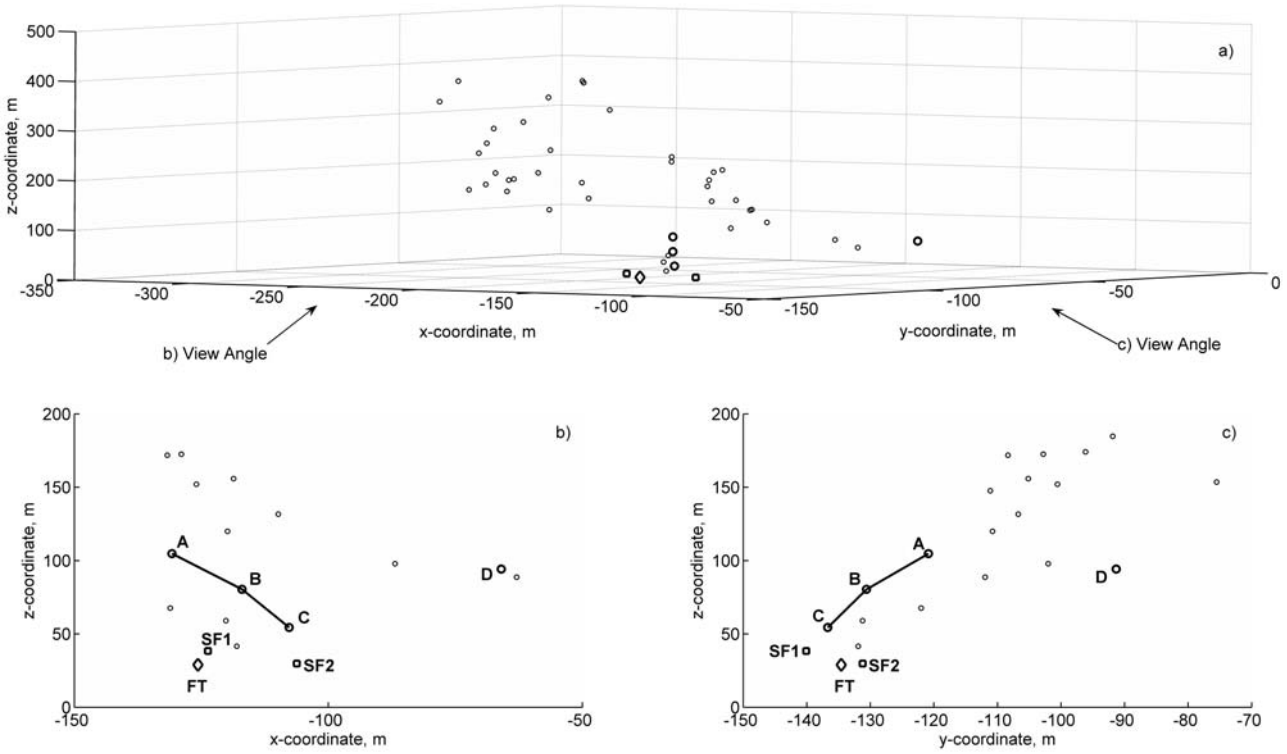

Figure 11. Visual representation for the first stroke of MSE-0704. The symbol notation is consistent with that previously used in Figures 4 and 9.

branches, resulting in a very complex waveform signature. Indeed, the second and third pulses of Group C (C2 and C3 in Table 2) appear to be more closely associated with Group D than Group C based on their TOA solutions. Hence, these two pulses are labeled in Table 2 with the clarifier ''BS'' to indicate they are part of and occurred before the step (LS) in Group D. If, however, we associate the second and third pulses of Group C with a separate step altogether, there is little change in the statistical analysis given later in section 4.2.

[30] From Figure 10, Group D can be identified as the final step of the leader phase. Although Group D was clearly associated with the connecting leader region, it apparently was not part of the connecting leader branch, which contained Groups A, B, and C. The time period between this final leader step and the start of the slow front, when we have previously observed LBs, did not produce any locatable events, although several stations did detect a few small pulses. Interestingly, these small pulses produced coincident X-rays at more stations than the previous leader step (Group D), the SF pulses, or the fast transition. The production of X-rays just prior to the slow front in this stroke may indicate a significant process in the attachment phase that occurs even in the absence of significant *dE*/*dt* activity. The locations provided by the TOA network for the SF and fast-transition *dE*/*dt* pulses are very tightly grouped except for some moderate spread ($\sim$20 m) in the *x* coordinates. It is noted that the *x* coordinate uncertainties (Table 2) for the events of this stroke were relatively high as a result of this stroke being nearly 200 m west of the network. Regardless of these larger uncertainties, the locations determined for the fast-transition and SF pulses were in excellent agreement with the video record.

[31] Examination of the *dE*/*dt* and X-ray waveforms revealed that only three stations detected X-rays following the leader phase. This fact is not particularly surprising considering the location of this stroke and the relatively high attenuation rate of X-rays with range ($\propto$[exp($-r$/120)]/r, as noted earlier). All three stations detected X-rays during the period suspected to contain a LB. Two of these three station detected X-rays associated with the SF pulses, and none of them detected X-rays with the fast-transition pulse. It is worth noting that this stroke provided the only instance in the data discussed here where a station (station 1) detected a stronger X-ray burst in association with a slow-front pulse (SF1) than it did with the LB, or the suspected LB in this case.

3.4. UF-0707

[32] Flash UF-0707, a rocket-and-wire triggered flash, was initiated on 31 July 2007 at approximately 19:36 UT. This flash consisted of an initial stage (as in all negative triggered lightning flashes, involving an upward positive leader, destruction of the triggering wire, its replacement with a plasma channel, and subsequent steady current flow between cloud and ground [e.g., *Rakov et al.*, 2003]) followed by two leader/return-stroke sequences, with each stroke terminating to the launcher mounted on the top of an 11 m tower. The focus in this section is the first of these two strokes. This stroke produced a peak channel-base current of approximately 45 kA (unusually high for a rocket-triggered lightning stroke, whose typical peak current is 10–15 kA [*Rakov and Uman*, 2003]) and was initiated by a dart-stepped leader. Additionally, the SF/fast-transition sequence, evident in both the *dE*/*dt* and channel-base current records, indicates that there was a pronounced attachment phase, not dissimilar to a natural-lightning first stroke. Video and photographic records for this stroke reveal that the downward leader was a single channel that only branched in the final 6–8 m above the launcher. Further, these optical records clearly indicate the presence of upward positive leaders extending from the launcher. The rare combination of data (TOA locations, electric and electric field-derivative records, channel-base current, and close optical records) available for this stroke provides a unique opportunity to study the stepped leader and the processes of the attachment phase.

[33] Two of the *dE*/*dt* waveforms recorded for this stroke are presented in Figure 12. A comparison of these waveforms with those previously presented for natural-lightning first strokes reveals that there are both similarities and differences. Like the natural-lightning waveforms, the groups of leader pulses in Figure 12 display a variety of shapes. Group A, for instance, exhibited the simple leader-step signature, while Groups B and C were complex leader steps involving many secondary pulses. Indeed, the amplitude and multiplicity of the secondary pulses gave these groups a distinct appearance, different from most of the leader groups that were observed in the natural-lightning strokes. However, some groups in the natural-lightning strokes, such as Groups H and I from Flash MSE-0604, did appear similar when viewed on an identical time scale. As with leader groups in the natural-lightning strokes, the secondary pulses in the leader groups of this stroke tended to originate from a similar location as the dominant pulse within the same group. The TOA locations for the pulses observed in Figure 12 are listed in Table 3. These pulses along with the rest of the pulses in the leader phase were used to produce the 3-D view of this stroke, which is presented in Figure 13. The symbol notation used in Figure 13 is the same as that previously used for the natural-lightning strokes. A number of the features observed in Figure 13 were confirmed via optical records. These features include the leader channel leaning southwest (decreasing *x* and *y*) away from the tower with increasing height as well as the change in channel trajectory at about 200 m altitude. This channel shape was likely established in the initial stage of the flash when the upward positive leader initiated from the wire-grounded rocket (typically at 200–300 m altitude [*Rakov and Uman*, 2003]) and propagated in a direction different from the original rocket trajectory. Additionally, the TOA locations do not indicate any branching of the leader, and the lowest sources from this stroke are over the eastern edge of the tower (left side of tower in Figure 13c).

[34] The fact that a dart-stepped leader precedes the return stroke of this flash while stepped leaders precede first strokes in natural lightning is responsible for some of the most notable differences between this and the natural-lightning strokes: (1) time interval between steps, (2) downward leader propagation speed, and (3) absence of significant branching. Thus far in this paper we have observed that pulses within each leader group tend to be very closely spaced, indicating that each group essentially corresponds to a leader step. Therefore, an estimate for the interstep interval can be obtained by simply observing the group spacing in the *dE*/*dt*

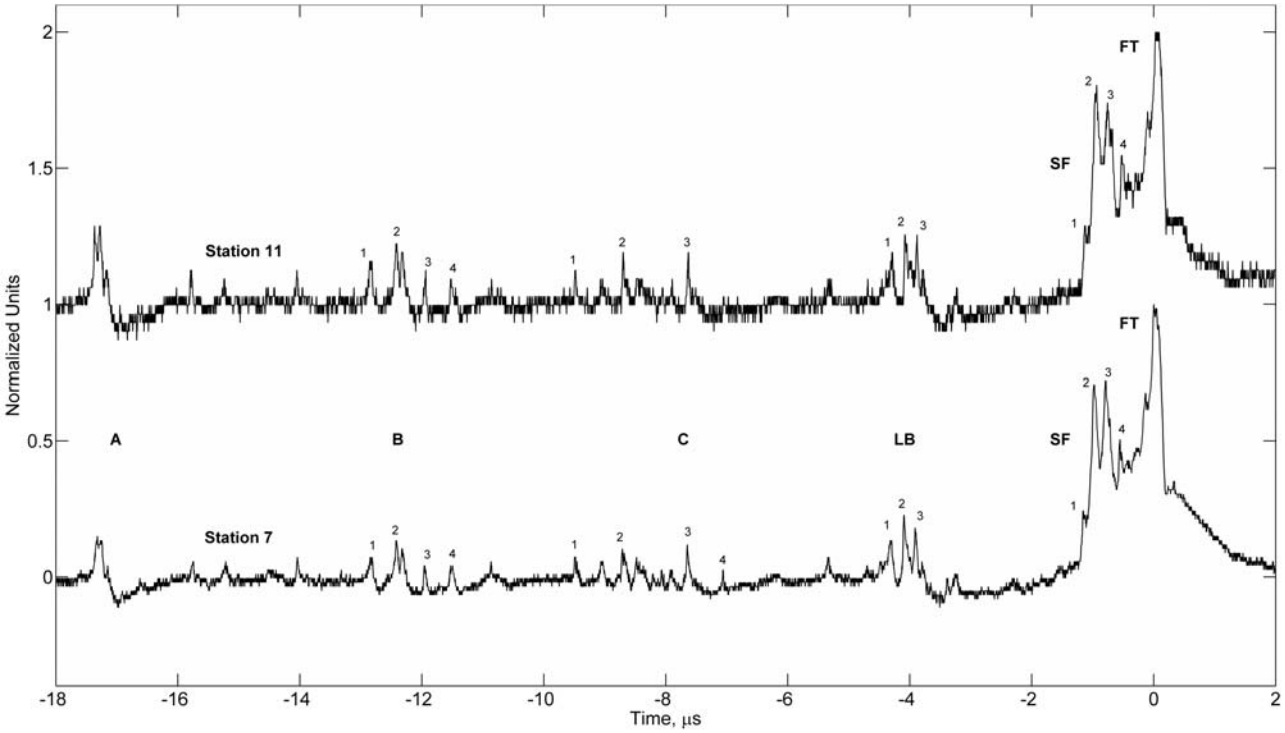

Figure 12. Two *dE*/*dt* waveforms for the first stroke in rocket-triggered flash UF-0707. Notice the unusual transition produced by the SF pulses.

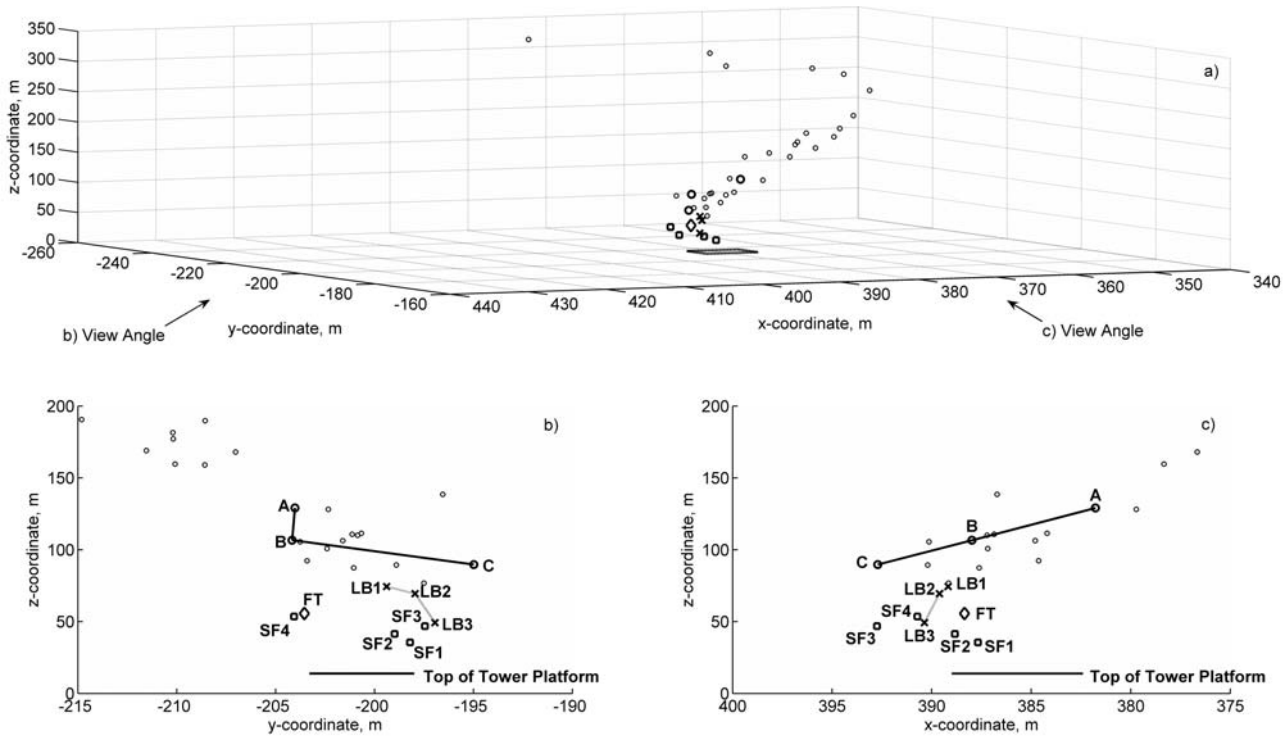

Figure 13. Visual representation for the first stroke in the rocket-triggered flash UF-0707. The symbol notation is consistent with that used for the natural strokes in Figures 4, 9, and 11. The rectangular outline below the downward leader indicates the location of the tower platform.

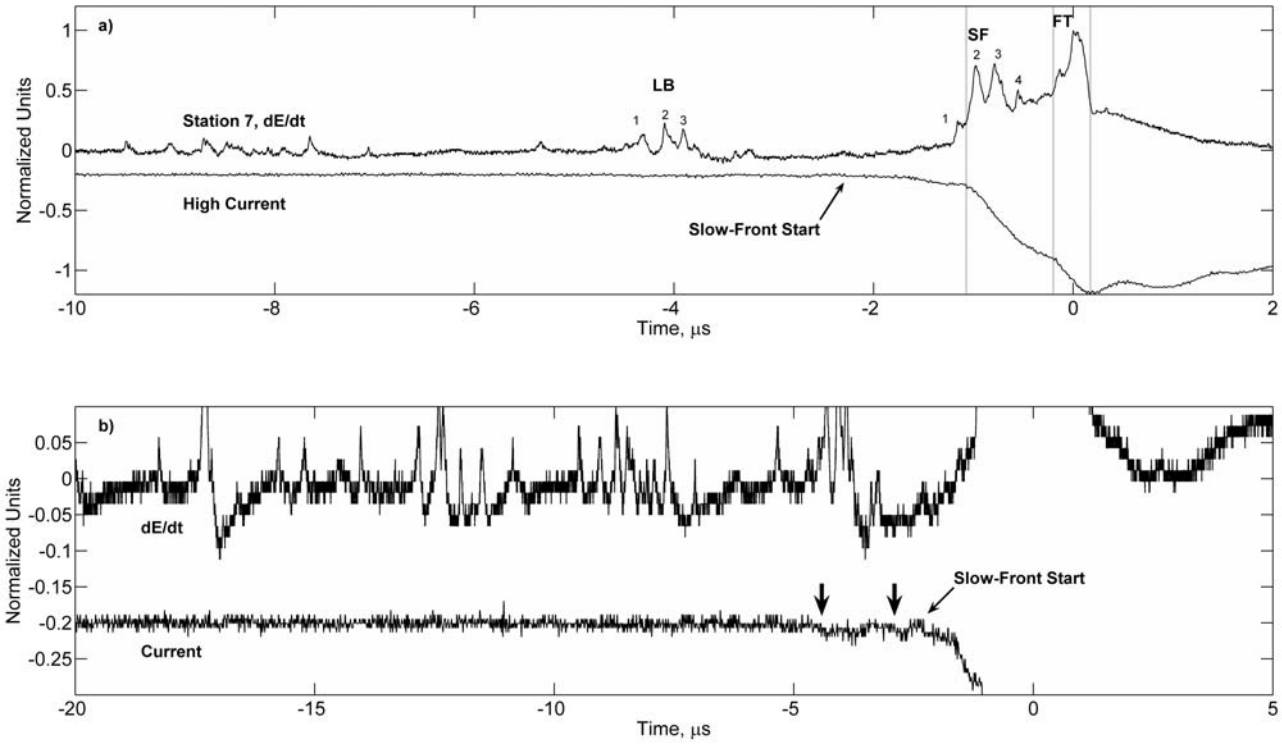

Figure 14. Comparison of station 7 *dE*/*dt* waveform and the channel-base current for rocket-triggered flash UF-0707. (a) The dotted lines highlight corresponding features in the two waveforms. The start of the slow front is indicated by the arrow marker. (b) An alternative view that highlights 200 A-level pulses in the current, which are indicated by the vertical arrows.

waveforms. For stepped leaders (Figures 2, 8, and 10), a typical interval between groups is 10–20 μs, with shorter intervals clearly being observed in Figure 2. However, consecutive groups in Figure 2 rarely belonged to the same leader branch (see Figure 4), implying that the typical interstep interval is probably more like 15–25 μs. On the other hand, Figure 12 indicates that the dart-stepped leader in this stroke has an interstep interval of approximately 4–5 μs. These values are in general agreement with the typical values reported for each of these leader types [*Rakov and Uman*, 2003]. Since neither the TOA locations nor optical records for this stroke indicate any branching of the downward leader (at least over 8 m or so above the launcher), all of the leader points identified in Figure 13 were used to calculate the downward velocity. On the basis of our linear regression method, the downward leader velocity was calculated to be 4.8×10^6 m s^{-1} with a determination coefficient between altitude and time of 0.99. The best fit results for this stroke are shown in the lower-right corner of Figure 6. This leader velocity is higher than any of the values previously reported for the stepped leaders, as expected, and is in good agreement with values typically reported for dart-stepped leaders [*Rakov and Uman*, 2003].

[35] A few microseconds after the final leader step (Group C in Figure 12), the *dE*/*dt* pulses identified as the LB occur. *Howard et al.* [2008] originally identified this group as a leader step. However, the following reasons indicate that these pulses may be more appropriately labeled as a LB: (1) the pulses within this group traversed significantly more altitude than the preceding leader groups and (2) the initial pulse of the LB began very near the preceding leader step, unlike previous leader steps in this stroke (see Table 3). Further, the X-ray records indicate that this group of pulses was one of the most significant X-ray events for this stroke and was certainly the most dominant following the leader phase, similar to LBs in the natural-lightning first strokes previously examined. The LB appears to have involved more than the three located peaks given in Table 3; however, some of the smaller pulses were not resolved well enough to provide locations. Following the LB in Figure 12, around −2.3 μs, there is a gradual rise in the *dE*/*dt* waveforms that continues until a sizable and rapid transition is produced by the slow-front pulses (comprised of SF1 and SF2), which is remarkably similar in shape to the actual fast-transition pulse of this stroke. Following slow-front pulses SF3 and SF4, the gradual rise resumes briefly until the onset of the fast transition (dominant pulse). Overall, the description of this stroke transitioning from the leader phase into the return stroke is very similar to that observed for the natural-lighting first strokes previously discussed, suggesting that the attachment phase for stepped and for dart-stepped leaders involves very similar processes.

[36] The current waveform for the first stroke of UF-0707 is presented in Figure 14 on two time scales along with the *dE*/*dt* waveform from station 7. The current exhibited a peak of approximately 45 kA, as noted previously, and complex slow front as opposed to the simple concave shape typically observed in the current and electric field waveforms of natural-lightning first strokes [e.g., *Weidman and Krider*, 1978; *Jerauld et al.*, 2007]. As with Figures 2, 3, 7, 8, 10,

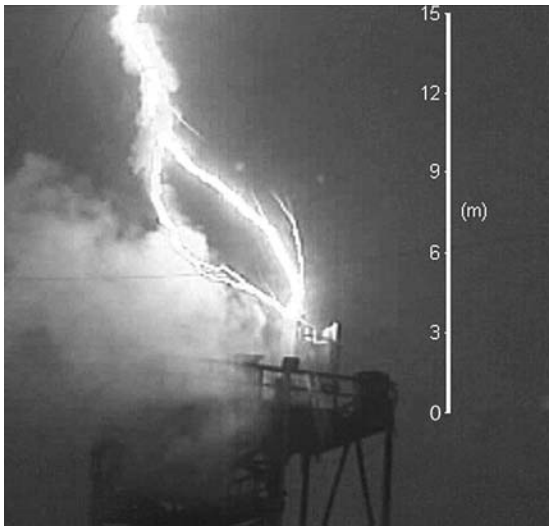

Figure 15. Single video frame imaging the first return stroke in flash UF-0707. There are two primary connections, with a subconnection visible in the lower primary channel. The image also reveals unconnected upward and downward leader branches. The height scale on the right indicates the height of the channel above the top of the Tower platform. The height of the channel termination point above the platform is 3.3 m.

12, 14, and 16–18, the *dE*/*dt* fast-transition peak is set to correspond to time zero. The alignment of the current waveform was based largely on the timing considerations obtained from the strike location and the known measurement delays. However, there were still a few hundred nanoseconds of ambiguity considering that the source of the current wave was likely located above the launcher, at the junction point of the downward and upward connecting leader [*Jerauld et al.*, 2007; *Willett et al.*, 1988, 1989; *Weidman et al.*, 1986; *Uman et al.*, 1973]. A reasonable and consistent time shift which accounts for this effect was introduced to the current waveform so that the start of the fast transition (end of the slow front), a noticeable feature, was aligned in both waveforms. The alignment of the end of the slow front and the beginning of the fast transition is indicated in Figure 14a by the middle dotted line. Interestingly, this alignment also produced matches in other features of the waveforms. The left dotted line indicates a correlation between the onset of the largest slow-front pulse (SF2) and a significant increase in channel-base current during the overall 2.1 μs slow front period. In fact, the left and middle dotted lines in Figure 14a reveal that both rapid transitions observed in the *dE*/*dt* waveform, because of the slow-front (SF1 and SF2) and fast-transition pulses, each corresponded to a significant increase in channel-base current. The rightmost dotted line indicates an alignment between the peak of the current waveform and the beginning of a shoulder following the *dE*/*dt* peak. This alignment is interesting because the waveforms found by *Jerauld et al.* [2007] for a rocket-triggered lightning stroke indicate that a similar shoulder in the close electric and magnetic field-derivative records corresponded with a zero crossing in the channel-base current-derivative measurement, which should correlate to a peak in the current record. In addition to these events, the start of the current SF, which we identify as the point where the waveform deflects from the zero level, is identified in Figures 14a and 14b by a slanted arrow marker. The initial current deflection can be seen in Figure 14b to correspond with the start of the gradual rise in the *dE*/*dt* waveform. The duration of the current slow front, from the arrow marker to the middle dotted line, was, as noted above, about 2.1 μs, which, interestingly, is identical to the mean value for the distant electric field slow front reported by *Weidman and Krider* [1978] for 34 subsequent strokes preceded by dart-stepped leaders. Our current SF amplitude to total peak ratio of about 0.71 is larger than the mean ratio of 0.4–0.5 for the distant electric field given by *Weidman and Krider* [1978], but it is nearly identical to the value of 0.74 for the current ratio given by *Jerauld et al.* [2007] for an unusual rocket-triggered stroke that was also preceded by a dart-stepped leader. Immediately preceding the current SF start shown in Figure 14b, a pair of bold vertical arrows denotes two pulses in the current record. Because of the relatively poor amplitude resolution of this measurement, we can only estimate from the 45 kA peak current that these pulses had peaks of at least several hundred amperes. Because these hundred-ampere pulses occurred before the sustained current of the slow front, the process responsible for these pulses appears to have involved stepping. An obvious candidate is an upward positive leader propagating in response to the descending negative leader. It may be significant that these pulses coincided with the LB. No previous pulses could be attributed to an upward leader, which is expected to have a duration of tens to a couple hundred microseconds [e.g., *Yokoyama et al.*, 1990; *Wang et al.*, 2001], and the sustained current of the slow front began immediately after the second current pulse. We note that upward positive leaders were imaged with this stroke, as the video frame in Figure 15 shows.

[37] At this point, it is interesting to consider the implications of the current and *dE*/*dt* records with regard to the observed channel geometry. Figure 15 presents a single frame from the Sony (DCR-TRV900) MiniDV camcorder located in Launch Control that imaged the first stroke of UF-0707. This image reveals that the downward leader branched approximately 6–8 m above the launcher top into two primary channels, each of which connected to the launcher. The left primary channel is itself composed of two channels (exhibits a split). There are also unconnected leader branches, directed both upward and downward. From the analysis of this stroke, we know that the postleader phase of the *dE*/*dt* records contained two rapid transitions; one was produced by the combined SF pulses and the other was the fast-transition pulse. Further, each of these transitions was preceded by a gradual rise in the *dE*/*dt* waveform and was also associated with a significant increase in channel-base current. These similarities, along with their proximity in location, imply that both events were the result of a common process, perhaps the connection between an upward and downward leader. Another interesting observation, although purely speculative, is that the rapid transition in the SF is immediately followed by another significant pulse (SF3) which may be associated with the sub-connection in the left primary channel. Clearly, it is important to understand the lightning physics to associate physical processes with waveform features, and that is one of the primary goals for this TOA network. Unfortunately,

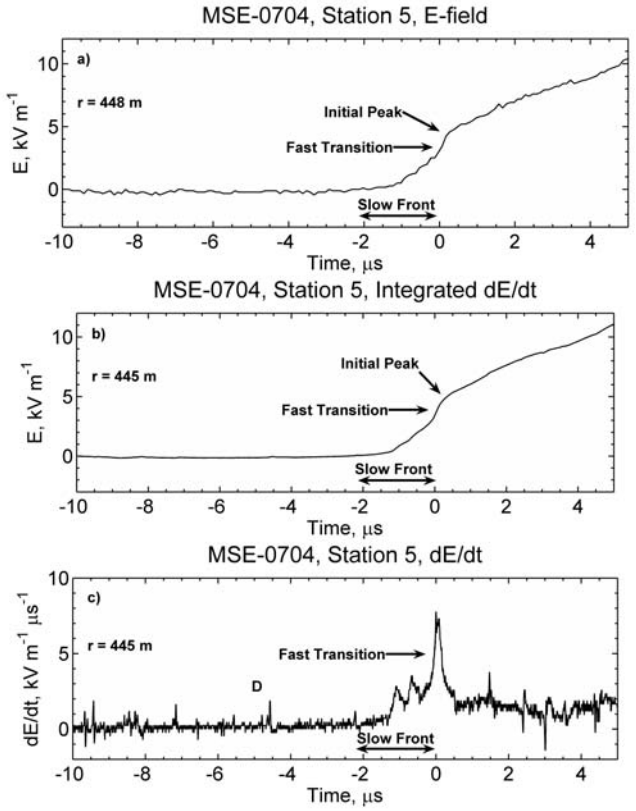

Figure 16. Comparison of (a) measured *E* field, (b) integrated *dE*/*dt*, and (c) *dE*/*dt* waveforms obtained at station 5 for MSE-0704.

the TOA network could not definitively identify the SF and fast-transition pulses as the source for the primary channel segments because of the altitude uncertainties in the TOA locations. However, the SF and fast-transition pulses were among the lowest sources located for this stroke. It is worth noting that the altitude uncertainties (Δz) for the sources in this stroke were uncharacteristically large because three *dE*/*dt* stations failed to record, resulting in a five-station solution. In particular, the two stations nearest to the tower, which are critical to the altitude determination [*Thomas et al.*, 2004], were among the three noncontributing stations. A discussion of the location errors for UF-0707 is found in section 4.4, including an argument that any sources potentially produced by the primary channel segments (within 8 m above the launcher top) would have been systematically located 15–25 m too high.

[38] The X-ray comparisons for this stroke were limited since only five *dE*/*dt* records were available. All five stations detected X-rays in association with the LB. One station detected X-rays during the SF pulses, and none of the stations detected X-rays in association with the fast-transition. As a final note regarding X-ray production and lightning processes, even if the 200 A current pulses in Figure 14b were the result of an upward positive leader, these occur simultaneously with *dE*/*dt* pulses (LB) that exhibited downward movement, so it is unclear if the observed X-rays are because of the LB process (likely given the association of X-rays with the LBs in the natural-lightning strokes and the fact that downward negative leader steps also produce X-rays) or the upward connecting leader.

4. Discussion and Conclusions

4.1. Electric Field and Field-Derivative Comparison

[39] One of the key features on which we have focused in this paper has been the transition from the leader phase to the return stroke. To this point, we have used the *dE*/*dt* waveforms to discuss these processes. However, researchers have more frequently used electric field measurements to study similar processes [e.g., *Weidman and Krider*, 1978], so it is worth comparing the *dE*/*dt* and *E* field records to correlate features in these two measurements. Figure 16 compares the measured electric field (Figure 16a), the time-integrated *dE*/*dt* (Figure 16b), and the *dE*/*dt* (Figure 16c) waveforms all obtained at station 5 for MSE-0704. This stroke is presented first because its *E* field record most closely resembles the "classical" description for a return-stroke electric field; an initial "slow front" having duration of 2–8 μs, followed by a "fast transition" to an initial peak, this peak not always being clearly identified in very close waveforms. Additionally, Figure 16 illustrates the excellent waveshape agreement between the directly measured *E* field and the integrated *dE*/*dt* obtained at the same station. For the waveforms of Figure 16, which were obtained at virtually the same distance, there is good agreement in the starting time and the duration of the slow front for each of the three waveforms. The slow front in both the directly measured *E* field and the integrated *dE*/*dt* waveforms exhibits the characteristic concave shape that is typically observed in first-stroke currents and distant *E* fields [e.g., *Weidman and Krider*, 1978; *Jerauld et al.*, 2007]. The SF pulses, which are clearly observed in the *dE*/*dt* waveform, correspond to only small inflections in the measured *E* field and integrated *dE*/*dt* waveforms.

[40] Figure 17 presents the *dE*/*dt* and integrated *dE*/*dt* waveforms from two stations for MSE-0604. Unfortunately, no directly measured *E* field waveforms were available for this stroke. Unlike the relatively simple structure observed in Figure 16 waveforms, the waveforms of Figure 17 exhibit more structure and highlight the varied appearance of features at different distances and the difficulty in identifying specific processes. The station 8 *dE*/*dt* waveform (Figure 17b) was obtained at a distance of 460 m from the ground-strike point, and the station 1 *dE*/*dt* waveform (Figure 17d) was obtained at distance of 195 m. The fast transition of the station 1 *dE*/*dt* waveform is saturated, so the corresponding integrated *dE*/*dt* waveform becomes distorted shortly after the transition labeled as T2. Both *dE*/*dt* waveforms in Figure 17 exhibit five distinct features: (1) the final leader step, Group K, (2) the LB pulses, (3) the SF pulses, (4) the start of a rapid transition (T1) to a shoulder, and (5) the start of a rapid transition (T2) to peak. The final leader step, Group K, is identifiable in the integrated *dE*/*dt* records of both stations and appears as a simple unipolar peak. Although this leader step is much larger in the *dE*/*dt* record at station 1 than at station 8, it is less noticeable in the station 1 integrated *dE*/*dt* waveform because of the large amplitude contribution of the return stroke. A similar effect is also observed in the integrated *dE*/*dt* records for both the LB and SF pulses. Although both integrated waveforms have an overall con-

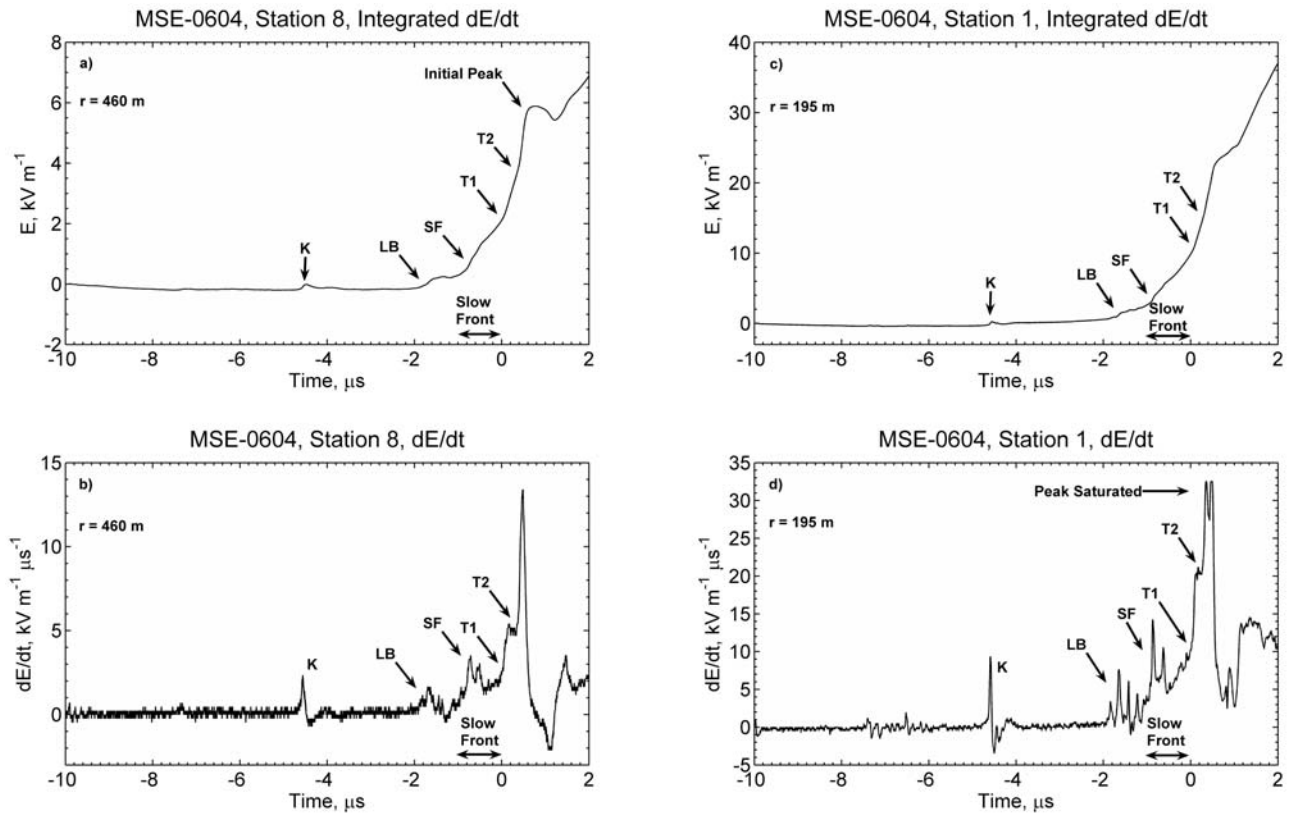

Figure 17. The *dE*/*dt* and integrated *dE*/*dt* waveforms from two stations for MSE-0604.

cave shape from the start of the LB to the time of the first transition (T1), the inflections caused by the LB and SF pulses are much more noticeable in the station 8 waveform. In fact, the station 8 integrated *dE*/*dt* waveform could be described as having a unipolar hump, because of the LB, followed by a slightly convex portion, because of the SF pulses. The two transitions (T1 and T2) labeled in Figure 17 waveforms highlight an interesting problem that occasionally arises when trying to characterize return-stroke waveforms; which of these two points should be considered as the start as the fast transition? On the other hand, some have noted for negative first return strokes, that when viewed on an expanded time scale, the slow front and fast transition in both *E* field and *dE*/*dt* often appear to be one continuous process, without a clear transition [*Murray et al.*, 2005; *Jerauld et al.*, 2008]. For the case in Figure 17, it is evident that the point at which that transition occurs is ambiguous. Since both T1 and T2 appear to be associated with the same transition, we have identified the first transition (T1) to be the start of the fast transition. Finally, we note that the point that we selected for the start of the slow front may not necessarily be consistent with other studies because we distinguish the LB from SF processes. If one were only looking at *E* field waveforms and were unaware that the LB was a separate process, it would likely be included as part of the slow front. Even if one is aware that there is a separate LB process, it may still be difficult to identify the end of the LB and the start of the slow front in an *E* field record.

[41] Figure 18 shows the integrated *dE*/*dt* (a) and *dE*/*dt* (b) waveforms from station 7 and the directly measured *E* field from station 4 (c) and station 9 (d) for UF-0707. The distance of each station from the launch tower is indicated in Figure 18. The key features in the Station 7 *dE*/*dt* waveform include the LB, the SF pulses, and the fast transition. Similar to MSE-0604, the LB can be seen to correspond with a unipolar hump or step in the integrated *dE*/*dt* and *E* field waveforms. As previously noted, two of the slow-front pulses (SF1 and SF2, Figure 12) generated a rapid transition that was very similar in appearance and amplitude to the fast transition. This "slow-front transition" resulted in some unusual characteristics in the electric field return-stroke waveforms. Examining the integrated *dE*/*dt* and E field waveforms, it cannot readily be determined exactly where the slow front begins and ends. Because the *dE*/*dt* and current waveforms for this stroke (Figure 14) appeared to have the same SF duration, the *dE*/*dt* record was used to determine the SF interval. When this time interval is examined in the integrated *dE*/*dt* and *E* field records, it looks nothing like a "classical" SF. In fact, the overall fast transition to field peak appears to involve two components, one occurring during the SF interval and the other occurring with the fast transition. The only feature distinguishing the two components of the overall transition is a small inflection in the *E* field (and integrated *dE*/*dt*), which corresponds to the slow rising interval observed between the two transitions in the *dE*/*dt* record. Although this multicomponent behavior of the fast transition has not been well-documented, it has been observed in previous studies. *Murray et al.* [2005] reported that their Type B events tended to exhibit an inflection point or additional peak within the fast transition of their integrated *dE*/*dt* waveforms for distant negative first strokes. *Jerauld et al.* [2008] reported on two positive strokes that struck ground 800 m apart (but

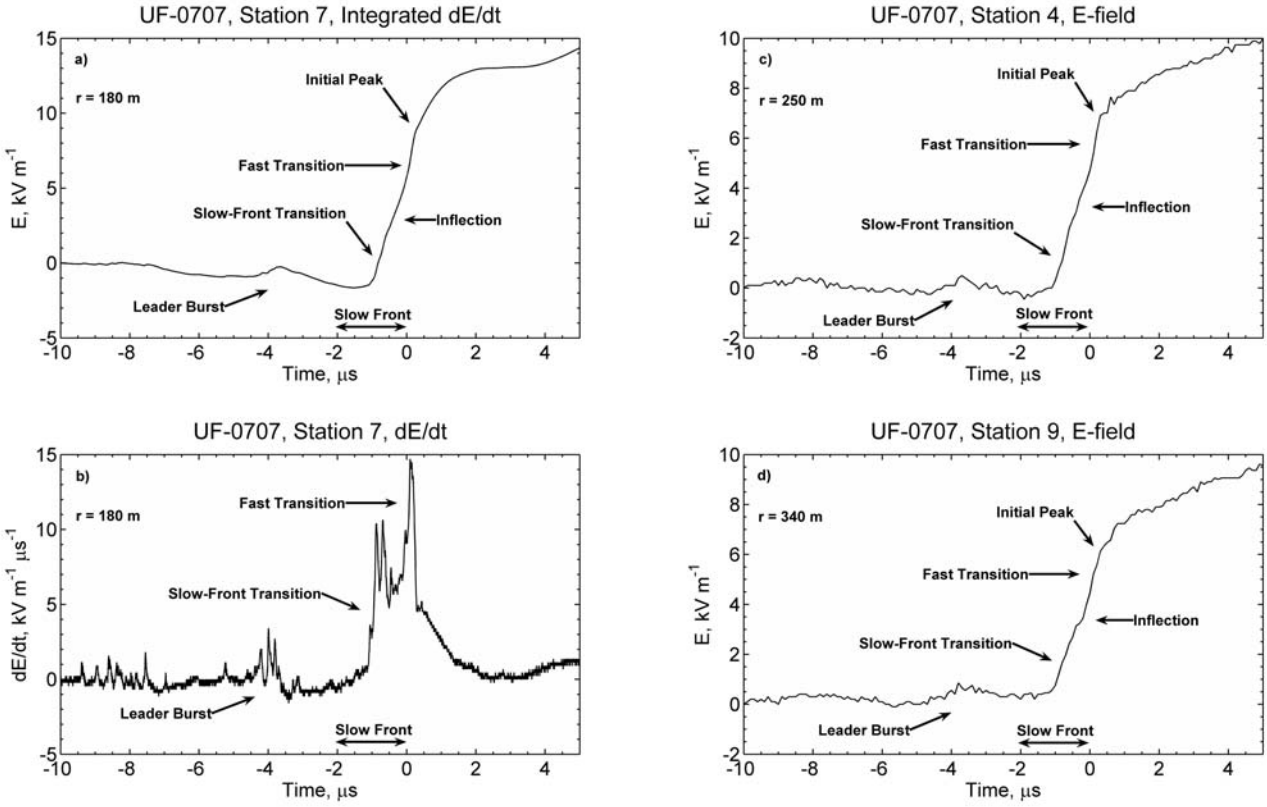

Figure 18. Comparison of (a) integrated *dE*/*dt* and (b) *dE*/*dt* waveforms at station 7 for UF-0707. *E* field waveforms from stations (c) 4 and (d) 9 are shown.

were in the same flash) which both exhibited a fast transition with two components. In both of these previous studies, similar to the data presented here, each component of the overall fast transition in the electric field corresponded to significant pulses in the *dE*/*dt* record. Finally, we note that each of the transitions (SF and fast) in the station 7 *dE*/*dt* record appears to have a front-side shoulder that is about one third to one half the peak value. This feature appears similar to that of the fast-transition observed for MSE-0604, but does not occur for the other strokes presented here. Although purely speculative, it is interesting that both of these strokes, UF-0707 and MSE-0604, were known to have attached to relatively tall objects, the launch tower and a tree, respectively.

4.2. Leader Phase

[42] In the *dE*/*dt* waveforms throughout this paper, the pulses were presented as groups, the reason being that pulses closely grouped in time were also found to be closely grouped in space, leading us to the conclusion that each group must correspond with a leader step. The structure of these groups was a dominant bipolar pulse, labeled as the leader step (LS), which may have smaller pulses within a few microseconds before (BS) or after (AS) it. We now examine the vertical spacing of these secondary pulses relative to the dominant pulse. Combining all leader groups listed in Tables 2 and 3 for both the natural and rocket-triggered flashes, we analyzed the vertical position of the secondary pulses relative to the dominant pulse as a function of whether they occurred before or after the dominant pulse in time. For the secondary pulses occurring before the leader step, BS pulses, we found that 8 out of 14 (57%) were located below the dominant pulse, with the average displacement for these 14 pulses being 0.4 m below the dominant pulse. On the other hand, seven out of nine (78%) secondary pulses occurring after the dominant pulse, AS pulses, were located below the dominant pulses, with an average displacement for these nine pulses being 7.2 m below the dominant pulse. Although this is not a large sample and the average vertical displacement is smaller than or equal to the vertical resolution of our TOA network, this analysis provides the first empirical insight into the stepping process of downward negative leaders in lightning. The data indicate that most electrical activity occurring just prior to the step is very near the new step location; while after the dominant step pulse (LS), the electrical activity is below the new step. From this result, we might infer that the stepping mechanism for a lightning leader is similar to that observed in the laboratory for some meters-long sparks [*Gorin et al.*, 1976; *Gallimberti et al.*, 2002; *Rakov and Uman*, 2003]. In a negative laboratory leader, a space stem develops in the streamer zone in front of the currently existing leader channel. The space stem gives rise to a bidirectional leader, which is positively charged toward the existing leader and negatively charged into the gap. When the space stem connects to the main leader channel, a relatively large step current is produced. Thereafter, an intense burst of corona streamers extends downward from the previous space stem (now part of the leader channel) to eventually form a new space stem. Assuming that a similar mechanism occurs in lightning leaders, perhaps it is the corona streamers, which initially extend both upward and

downward from the space stem (creating the BS pulses preceding the main leader pulse) and later extend below the new leader step (creating the AS pulses following the leader step), that are responsible for the secondary pulses in leader steps and their observed vertical distributions. Because streamer tips are a currently favored source for X-ray production [*Dwyer*, 2004; *Moss et al.*, 2006, *Rahman et al.*, 2008; *Dwyer et al.*, 2008], it is also worth noting that the time of occurrence for locatable X-ray emissions was found to follow the leader-step electric field change by $\sim$1 μs with some evidence of weaker X-ray emission just prior to the step [*Howard et al.*, 2008], perhaps further evidence that the stepping mechanism of the negative-lightning leader is similar to that observed in the laboratory.

4.3. Postleader Phase

4.3.1. Leader Burst

[43] A burst of pulses that occurs near or at the beginning of the slow front has been previously reported by *Murray et al.* [2005] for distant (radiation field) *dE*/*dt* waveforms from negative first strokes, as well as by *Jerauld et al.* [2007, 2008] for close negative first-stroke *dE*/*dt* waveforms. *Murray et al.* [2005] found that 75 of 131 events (or 57%) exhibited a LB in the interval from -9 to -4 μs prior to the dominant *dE*/*dt* pulse. Further, they acknowledged that many of the pulses observed between -4 to -1 μs of the dominant peak may have also been the result of LBs. To date, there is no information or explanation for the LB pulses. We have shown: (1) that their location is below the steps of the previous leader phase, (2) that they are associated with a rapid and significant downward movement, not typically observed with preceding leader steps (the LB may also cover significant horizontal distances or involve simultaneous activity by the downward leader and upward connecting leader), (3) that the LB produces a significant amount of X-rays, and (4) that the LB *dE*/*dt* feature corresponds to a hump or step in the electric field waveform (the latter observation is supported by the waveforms of *Murray et al.* [2005] and *Jerauld et al.* [2008]).

[44] *Wang et al.* [2001] studied upward positive leaders in downward negative lightning using the ALPS imaging system and a correlated *E* field measurement. In one particular stroke, located approximately 2 km from their instruments, the *E* field record showed a small unipolar pulse with a risetime of 0.5 μs and duration less than 2 μs occurring just prior to the slow front. This electric field pulse temporally coincided with a small optical signal observed only in the lowest channel of the ALPS system ($\sim$35 m above ground). Prior to this pulse, an upward leader had already extended up to a height of 88 m over a time of 53 μs, giving it an average upward speed of 1.7×10^6 m s^{-1}. The upward leader was initiated when the downward leader, having an average speed of 4×10^6 m s^{-1}, was about 300 m above ground. *Wang et al.* [2001] could not provide an explanation for the unipolar electric field pulse; but the low altitude of the correlated optical signal and the timing and shape of the electric field pulse, consistent with the data presented here, suggest that the pulse resulted from a LB. If we continue this line of reasoning, the work of *Wang et al.* [2001] shows that the LB produces an observable light emission and occurs after the initiation of the upward positive leader.

4.3.2. Slow-Front Pulses and the Fast Transition

[45] Slow front pulses have been previously reported by *Murray et al.* [2005] and *Jerauld et al.* [2007]. Modeling results provided by *Jerauld et al.* [2007] for an unusual rocket-triggered lightning indicated that the radiation field from the SF pulses looked similar to but smaller in amplitude than the fast-transition radiation field. Additionally, the distant radiation *dE*/*dt* pulses observed in Type B and Type C events by *Murray et al.* [2005] often appeared very similar to the dominant *dE*/*dt* pulse, indicating that the SF and fast-transition pulses may be produced by a similar physical mechanism. No explanations presently exist for these pulses, although we have evidence for the physical mechanism of the slow front itself [*Jerauld et al.*, 2007]. On the basis of the locations given for the four strokes here, we see that the SF pulses have a similar location as the fast transition, and even as the AFT pulse of MSE-0703. Unlike the LB pulses, these do not suggest a consistent pattern of motion. On the basis of the discussion presented by *Jerauld et al.* [2008] for a positive stroke electric field-derivative waveform, records presented by *Murray et al.* [2005], and our present data, we can reasonably conclude that the difference in SF and fast-transition pulses is simply terminology. We located the SF pulses for MSE-0604 away from the main leader activity and very near the tree that was struck. The fast transition was not located for this flash, but evidence from other strokes indicates that the SF and FT pulses are located in the same general area. Because the duration of the upward positive leader is expected to be some tens to hundreds of microseconds in duration, we do not expect the SF pulses to be the result of propagation of this leader. Additionally, in the SF transition exhibited by the rocket-triggered flash UF-0707, the channel-base current rose, coincident with the SF transition, to a value near 20 kA (Figure 14). That value seems unreasonably large for an unconnected upward leader, which argues that a connection had already occurred. At the time of the actual fast transition, the current rises sharply again. Two channels are observed in the photograph of UF-0707 (Figure 15), which may indicate that each transition corresponded to a separate channel. One of the channels had a subconnection, which may be related to the large pulse (SF3) observed immediately after the SF transition peak (Figure 12). From the *E* field records, both transitions appear similar (Figure 18). If the fast transition corresponds to a connection, it is a logical extension that the first transition, which actually resulted in a larger current increase, was also a connection. It may be that all slow front pulses correspond to a connection. Indeed, if the electric field was not always dominated by the fast transition, the relatively rapid electric field changed caused by the SF *dE*/*dt* pulses may appear to be like the fast transition in the electric field on a smaller amplitude scale. We may conclude that if one integrates the SF *dE*/*dt* pulse or pulses, one generally obtains a smaller electric field slope than if one integrates the larger fast-transition pulse, but sometimes the difference in slope is small, and hence the identification of SF and fast-transition *dE*/*dt* pulses is primarily determined by their relation in time.

4.4. Discussion of TOA Errors

[46] The uncertainty in individual source locations is dependent on factors such as the geometry of the network, the number of stations used, and the location of the source

itself; therefore, it is very difficult to provide a simple, singular metric to describe the accuracy of the solutions. Perhaps the most encompassing description for the network accuracy is the RMS timing uncertainty that exists for each measurement [*Thomas et al.*, 2004]. This quantity, which is assumed constant and the same for each station, is used by the nonlinear least squares Marquardt algorithm to calculate the Chi-square goodness of fit value. Note, however, that this value is not necessarily known a priori. Once this value is known, the location uncertainty for individual source locations can be obtained through simple geometric calculations or Monte Carlo analysis [*Thomas et al.*, 2004; *Koshak et al.*, 2004]. According to *Thomas et al.* [2004], the most accurate method for determining the timing uncertainty is to compare the distribution of reduced Chi-square values obtained for the solutions with the theoretical distributions. Regardless of the value initially chosen for the timing uncertainty, the reduced Chi-square values are readily scaled to correspond with any value of timing uncertainty by using a simple scaling factor. Unfortunately, this method requires that many source locations be determined for each degree of freedom, i.e., the timing uncertainty is dependent on the number of stations used, and separate comparisons must be made for solutions obtained with different numbers of stations. Because we record only several flashes per year with perhaps tens to a hundred sources located per stroke, a sufficient number of solutions is not currently available for such an analysis. To make some approximation for the timing uncertainty of our network, we examined the horizontal uncertainties (Δx and Δy) returned in the covariance matrix for actual lightning sources that were relatively central to the network, primarily the sources of UF-0707 and the sources used for calculating the leader speed of MSE-0604 (Figure 5). These errors should be largely independent of source altitude if the sources are surrounded by the network stations. We then ran Monte Carlo simulations for source locations similar to these two strokes at several altitudes and different timing errors that ranged from 4 to 30 ns (standard deviation of an assumed normal distribution whose mean is zero). The covariance estimates obtained for the test points in the Monte Carlo analysis, which introduced known distributions of timing error, were then compared with the lightning data to estimate the RMS timing uncertainty of the network. The Monte Carlo analysis utilized the same five-station combination that was used with the UF-0707 data and conservatively assumed the eight-station combination with the MSE-0604 data (i.e., smaller station combinations require a lesser value of timing error to get similar results as the eight-station combination with larger timing error). For both strokes, covariance estimates of the horizontal errors from the lightning data were best matched using timing errors of 6–10 ns in the Monte Carlo analysis. This range of values was secondarily supported by the fact that the reduced Chi-square values for the lightning sources used in this analysis had to be scaled to a timing error of approximately 10 ns to produce a mean value of 1.

[47] As previously noted, the timing error can be used to determine location accuracy for specific source locations and station combinations. Because the source locations for the SF and fast-transition pulses in the rocket-triggered stroke, UF-0707, did not descend to the top of the launcher as we might expect (Figures 13 and 15), we performed Monte Carlo simulations to examine the vertical error distributions for a source located 4 m above the launcher (approximately half the height of apparent attachment region, Figure 15) that was degraded by our estimated timing errors (6–10 ns) and located by the same 5 stations as UF-0707. Interestingly, our range of timing errors resulted in vertical error distributions with means of +15 to +25 m and standard deviations of 22–29 m. These positive mean values indicate that the altitude of a source at that position would have likely been overestimated by that range of values, and hence the final sources located from UF-0707 were potentially lower than the altitudes listed in Table 3. Indeed, if the SF and fast-transition pulses of UF-0707 were corrected by 15–25 m, they would be much closer to the top of the launcher, supporting the idea that the SF and fast-transition pulses were responsible for the primary channels imaged with this stroke (Figure 15). This systematic overestimation of the source height quickly disappears with increasing altitude, as the mean of the vertical error distribution falls to <1 m at approximately 50 m above the launcher (or about 67 m in the local coordinate system); therefore, sources located during the leader phase of this stroke are not expected to have suffered significantly from this effect. Finally, it is interesting to note that a source in the same position (4 m above the launcher) but located using all eight stations would be expected to have a vertical error distribution with a mean less than 5 m and a standard deviation less than 15 m.

5. Summary

[48] The leader and attachment phases of three first strokes in natural cloud-to-ground lightning and one rocket-triggered-lightning stroke, which was initiated by a dart-stepped leader, have been analyzed using an eight-station network of colocated and time-synchronized *dE*/*dt* antennas and X-ray detectors. The TOA locations of the leader-phase *dE*/*dt* pulses indicate that individual leader steps result from a series of electrical breakdowns and may exhibit features similar to those of leader steps in long air gap discharges observed in the laboratory. Further, the downward progression of the leader pulses within several hundred meters of ground was well fit by a linear regression, indicating velocities between 3.6×10^5 and 9.0×10^5 m s^{-1} for the natural-lightning strokes and 4.8×10^6 m s^{-1} for the rocket-triggered-lightning stroke. In addition, three postleader processes, all of which were located beneath the steps of the leader phase, have been identified: (1) LB, (2) SF pulses, and (3) the fast transition. All three of these processes were associated with X-ray production although the most significant X-rays were associated with the LB and decreased with subsequent postleader processes. The LB exhibited rapid and significant downward movement, not typically observed with the preceding leader steps (the LB may also cover significant horizontal distances or involve simultaneous progression of the downward and upward connecting leaders), and it corresponded to a hump or step that occurred just prior to the slow front in the electric field waveform. The SF and fast-transition pulses had similar TOA locations and appeared to be the result of a similar process, involving multiple connections between upward and downward leader branches. SF pulses of significant magnitude appear to contribute to the overall fast transition in the corresponding electric field return-stroke waveform.

[49] **Acknowledgments.** The research reported here was funded in part by the DARPA (HR0011-08-1-0088), the NSF (ATM 0420820, ATM 0607885, ATM 0003994, ATM 0346164, and ATM 0133773), and the FAA (99-G-043).

References

Berger, K., and E. Vogelsanger (1966), Photographische blitzuntersuchungen de jahre 1955–1965 auf dem Monte San Salvatore, *Bull. Schweiz. Elektrotech. Ver.*, *57*, 599–620.

Berger, K., R. B. Anderson, and H. Kroninger (1975), Parameters of lightning flashes, *Electra*, *80*, 23–37.

Biagi, C. J., D. M. Jordan, M. A. Uman, J. D. Hill, W. H. Beasley, and J. Howard (2009), High-speed video observations of rocket-and-wire initiated lightning, *Geophys. Res. Lett.*, *36*, L15801, doi:10.1029/2009GL038525.

Cooray, V., and S. Lundquist (1982), On the characteristics of some radiation fields from lightning and their possible origin in ground flashes, *J. Geophys. Res.*, *87*(C13), 11,203–11,214, doi:10.1029/JC087iC13p11203.

Dwyer, J. R. (2004), Implications of X-ray emission from lightning, *Geophys. Res. Lett.*, *31*, L12102, doi:10.1029/2004GL019795.

Dwyer, J. R., et al. (2003), Energetic radiation produced during rocket-triggered lightning, *Science*, *299*(5607), 694–697, doi:10.1126/science.1078940.

Dwyer, J. R., et al. (2004), Measurements of X-ray emission from rocket-triggered lightning, *Geophys. Res. Lett.*, *31*, L05118, doi:10.1029/2003GL018770.

Dwyer, J. R., et al. (2005), X-ray bursts associated with leader steps in could-to-ground lightning, *Geophys. Res. Lett.*, *32*, L01803, doi:10.1029/2004GL021782.

Dwyer, J. R., Z. Saleh, H. K. Rassoul, D. Concha, M. Rahman, V. Cooray, J. Jerauld, M. A. Uman, and V. A. Rakov (2008), A study of X-ray emission from laboratory sparks in air at atmospheric pressure, *J. Geophys. Res.*, *113*, D23207, doi:10.1029/2008JD010315.

Eriksson, A. J. (1978), Lightning and tall structures, *Trans. S. Afr. Inst. Electr. Eng.*, *69*, 238–252.

Gallimberti, I., G. Bacchiega, A. Bondiou-Clergerie, and P. Lalande (2002), Fundamental processes in long air gap discharges, *C. R. Phys.*, *3*, 1335–1359, doi:10.1016/S1631-0705(02)01414-7.

Golde, R. H. (1967), The lightning conductor, *J. Franklin Inst.*, *283*, 451–477, doi:10.1016/0016-0032(67)90597-2.

Gorin, B. N., V. I. Levitov, and A. V. Shkilev (1976), Some principles of leader discharge of air gaps with a strong non-uniform field, *IEE Conf. Publ.*, *143*, 274–278.

Gurevich, A. V. (1961), On the theory of runaway electrons, *Sov. Phys. JETP Engl. Transl.*, *12*, 904–912.

Gurevich, A. V., and K. P. Zybin (2001), Runaway breakdown and electric discharges in thunderstorms, *Phys. Uspekhi*, *44*, 1119–1140, doi:10.1070/PU2001v044n11ABEH000939.

Gurevich, A. V., G. M. Milikh, and R. A. Roussel-Duprè (1992), Runaway electron mechanism of air breakdown and preconditioning during a thunderstorm, *Phys. Lett. A*, *165*, 463–468, doi:10.1016/0375-9601(92)90348-P.

Hagenguth, J. H. (1947), Photographic study of lightning, *Trans. Am. Inst. Electr. Eng.*, *66*, 577–585, doi:10.1109/T-AIEE.1947.5059482.

Howard, J., M. A. Uman, J. R. Dwyer, D. Hill, C. Biagi, Z. Saleh, J. Jerauld, and H. K. Rassoul (2008), Co-location of lightning leader X-ray and electric field change sources, *Geophys. Res. Lett.*, *35*, L13817, doi:10.1029/2008GL034134.

Jerauld, J. (2007), Properties of natural cloud-to-ground lightning inferred from multiple-station measurements of close electric and magnetic fields and field derivatives, Ph.D. dissertation, Univ. of Florida, Gainesville, Fla. (Available at http.//purl.fcla.edu/fcla/etd/UFE0021279.)

Jerauld, J., M. A. Uman, V. A. Rakov, K. J. Rambo, and G. H. Schnetzer (2007), Insights into the ground attachment process of natural lightning gained from an unusual triggered-lightning, *J. Geophys. Res.*, *112*, D13113, doi:10.1029/2006JD007682.

Jerauld, J., M. A. Uman, V. A. Rakov, K. J. Rambo, D. M. Jordan, and G. H. Schnetzer (2008), Electric and magnetic fields and field derivatives from lightning stepped leaders and first return strokes measured at distances from 100 to 1000 m, *J. Geophys. Res.*, *113*, D17111, doi:10.1029/2008JD010171.

Jordan, D. M., V. P. Idone, V. A. Rakov, M. A. Uman, W. H. Beasley, and H. Jurenka (1992), Observed dart leader speed in natural and triggered lightning, *J. Geophys. Res.*, *97*, 9951–9957, doi:10.1029/92JA01458.

Koshak, W. J., et al. (2004), North Alabama Lightning Mapping Array (LMA): VHF source retrieval algorithm and error analysis, *J. Atmos. Oceanic Technol.*, *21*, 543–558, doi:10.1175/1520-0426(2004)021<0543:NALMAL>2.0.CO;2.

Lehtinen, N. G., T. F. Bell, and U. S. Inan (1999), Monte Carlo simulation of runaway MeV electron breakdown with application to red sprites and terrestrial gamma ray flashes, *J. Geophys. Res.*, *104*(A11), 24,699–24,712, doi:10.1029/1999JA900335.

Lin, Y. T., M. A. Uman, J. A. Tiller, R. D. Brantley, W. H. Beasley, E. P. Krider, and C. D. Weidman (1979), Characterization of lightning return stroke electric and magnetic fields from simultaneous two-station measurements, *J. Geophys. Res.*, *84*, 6307–6314, doi:10.1029/JC084iC10p06307.

Maier, L., C. Lennon, T. Britt, and S. Schaefer (1995), LDAR System Performance and Analysis, paper presented at the 6th Conference on Aviation Weather Systems, Am. Meteorol. Soc., Boston.

Master, M. J., M. A. Uman, W. H. Beasley, and M. Darveniza (1984), Lightning induced voltages on power lines: Experiment, *IEEE Trans. Power Apparatus Syst.*, *103*, 2519–2529, doi:10.1109/TPAS.1984.318406.

Moore, C. B., K. B. Eack, G. D. Aulich, and W. Rison (2001), Energetic radiation associated with lightning stepped-leaders, *Geophys. Res. Lett.*, *28*, 2141–2144, doi:10.1029/2001GL013140.

Moss, G. D., V. P. Pasko, N. Liu, and G. Veronis (2006), Monte Carlo model for analysis of thermal runaway electrons in streamer tips in transient luminous events and streamer zones of lightning leaders, *J. Geophys. Res.*, *111*, A02307, doi:10.1029/2005JA011350.

Murray, N. D., E. P. Krider, and J. C. Willett (2005), Multiple pulses in *dE*/*dt* and the fine-structure of E during the onset of first return strokes in cloud-to-ocean lightning, *Atmos. Res.*, *76*, 455–480, doi:10.1016/j.atmosres.2004.11.038.

Orville, R. E. (1968), Photograph of a close lightning flash, *Science*, *162*, 666–667, doi:10.1126/science.162.3854.666.

Orville, R. E., and V. P. Idone (1982), Lightning leader characteristics in the Thunderstorm Research International Program (TRIP), *J. Geophys. Res.*, *87*, 11,177–11,192, doi:10.1029/JC087iC13p11177.

Poehler, H. A., and C. L. Lennon (1979), Lightning Detection and Ranging System (LDAR): System and performance objectives, *Tech. Rep. TM-74105*, NASA, Kennedy Space Center, Fla.

Rahman, M., V. Cooray, N. A. Ahmad, J. Nyberg, V. A. Rakov, and S. Sharma (2008), X-rays from 80-cm long sparks in air, *Geophys. Res. Lett.*, *35*, L06805, doi:10.1029/2007GL032678.

Rakov, V. A., and M. A. Uman (2003), *Lightning: Physics and Effects*, Cambridge Univ. Press, New York.

Rakov, V. A., D. E. Crawford, V. Kodali, V. P. Idone, M. A. Uman, G. H. Schnetzer, and K. J. Rambo (2003), Cutoff and reestablishment of current in rocket-triggered lightning, *J. Geophys. Res.*, *108*(D23), 4747, doi:10.1029/2003JD003694.

Rison, W., R. J. Thomas, P. R. Krehbiel, T. Hamlin, and J. Harlin (1999), A GPS-based three-dimensional lightning mapping system: Initial observations in central New Mexico, *Geophys. Res. Lett.*, *26*, 3573–3576, doi:10.1029/1999GL010856.

Saleh, Z., J. R. Dwyer, J. Howard, H. Rassoul, M. Bakhtiari, M. A. Uman, D. Concha, M. Stapleton, D. Hill, and C. Biagi (2009), Properties of the X-ray emission from rocket-triggered lightning as measured by the Thunderstorm Energetic Radiation Array (TERA), *J. Geophys. Res.*, *114*, D17210, doi:10.1029/2008JD011618.

Schonland, B. F. J. (1956), The lightning discharge, *Handb. Phys.*, *22*, 576–628.

Thomas, R. J., P. R. Krehbiel, W. Rison, S. J. Hunyady, W. P. Winn, T. Hamlin, and J. Harlin (2004), Accuracy of the Lightning Mapping Array, *J. Geophys. Res.*, *109*, D14207, doi:10.1029/2004JD004549.

Thomson, E. M., P. J. Medelius, and S. Davis (1994), A system for locating the sources of wideband *dE*/*dt* from lightning, *J. Geophys. Res.*, *99*, 22,793–22,802.

Uman, M. A., D. K. McLain, R. J. Fisher, and E. P. Krider (1973), Currents in Florida lightning return strokes, *J. Geophys. Res.*, *78*, 3530–3537, doi:10.1029/JC078i018p03530.

Visacro, S., A. Soares Jr., M. A. O. Schroeder, L. C. Cherchiglia, and V. J. deSousa (2004), Statistical analysis of lightning current parameters: Measurements at Morro do Cachimbo Station, *J. Geophys. Res.*, *109*, D01105, doi:10.1029/2003JD003662.

Wang, D., V. A. Rakov, M. A. Uman, N. Takagi, T. Watanabe, D. E. Crawford, K. J. Rambo, G. H. Schnetzer, R. J. Fisher, and Z. I. Kawasaki (1999), Attachment process in rocket-triggered lightning strokes, *J. Geophys. Res.*, *104*, 2143–2150, doi:10.1029/1998JD200070.

Wang, D., M. Chen, N. Takagi, and T. Watanabe (2001), Correlated submicrosecond E field and high-speed image of the natural lightning attachment process, paper presented at 2001 International Aerospace and Ground Conference on Lightning and Static Electricity, Soc. of Autom. Eng., Seattle, Wash.

Weidman, C. D., and E. P. Krider (1978), The fine structure of lightning return stroke wave forms, *J. Geophys. Res.*, *83*(C12), 6239–6247, doi:10.1029/JC083iC12p06239.

Weidman, C. D., J. Hamelin, C. Leteinturier, and L. Nicot (1986), Correlated current-derivative (*dI*/*dt*) and electric field-derivative (*dE*/*dt*) emitted by

triggered lightning, paper presented at 1986 International Aerospace and Ground Conference on Lightning and Static Electricity, U.S. Air Force, Dayton, Ohio.

Willett, J. C., V. P. Idone, R. E. Orville, C. Leteinturier, A. Eybert-Berard, L. Barret, and E. P. Krider (1988), An experimental test of the "transmission-line model" of electromagnetic radiation from triggered lightning return strokes, *J. Geophys. Res.*, *93*, 3867–3878, doi:10.1029/JD093iD04p03867.

Willett, J. C., J. C. Bailey, V. P. Idone, A. Eybert-Berard, and L. Barret (1989), Submicrosecond intercomparison of radiation fields and currents in triggered lightning return strokes based on the transmission-line model, *J. Geophys. Res.*, *94*, 13,275–13,286, doi:10.1029/JD094iD11p13275.

Yokoyama, S., K. Miyake, T. Suzuki, and S. Kanao (1990), Winter lightning on Japan Sea Coast–development of measuring system on progressing feature of lightning discharge, *IEEE Trans. Power Delivery*, *5*, 1418–1425, doi:10.1109/61.57984.

C. Biagi, D. Hill, J. Howard, V. A. Rakov, and M. A. Uman, Department of Electrical and Computer Engineering, University of Florida, Gainesville, FL 32611, USA. (ironjoe@ufl.edu)

J. Dwyer, H. Rassoul, and Z. Saleh, Department of Physics and Space Sciences, Florida Institute of Technology, Melbourne, FL 32901, USA.

J. Jerauld, Raytheon Missile Systems, 1151 E. Hermans Rd., Tucson, AZ 85756-9367, USA.